A Photoluminescence Study of Indium Implanted Silicon

A thesis for the degree of

Master of Science

Submitted to

Dublin City University

by

Thomas Bernard Kehoe B.Sc.

Research Supervisor

Dr. Martin Henry

School of Physical Sciences

Dublin City University

August 1993

Declaration

I hereby certify that this material, which I now submit for assessment on the programme of study leading to the award of Master of Science is entirely my own work and has not been taken from the work of others save and to the extent that such work has been cited and acknowledged within the text of my work

Signed Thomas Kehoe Date 10th. Nov. '93

Thomas Kehoe

Contents

page

Chapter 4 Results

Chapter 5 Discussion and conclusions

Abstract

The results of a photoluminescence (PL) study of indium implanted silicon are presented When silicon implanted with indium is annealed in the temperature range 400°C to 700°C a sharp no-phonon line at 1096 6 ± 0 1 meV with an associated phonon sideband is produced in the PL spectra Using uniaxial stress perturbation techniques the no-phonon line is identified as an A to A transition at a centre with trigonal symmetry The shift rates for the line under stress are found to be nonlinear, indicating that some interaction with a nearby excited state is occurring Transitions from this state are not directly observed Evidence suggests that the luminescence arises from the recombination of excitons bound to an electrically neutral indium-implantation damage related centre, and that these exciton states are conduction band associated or donor-like in nature This centre is shown to be similar to one of three defects observed by Wichert et al [1], using the perturbed angular correlation (PAC) spectroscopy technique, in silicon implanted with the radioactive indium isotope, indium-111

The benefits of PL as a complementary technique to PAC and other nuclear techniques, and of radioactive implants to PL spectroscopy, are briefly outlined

[1] Th Wichert, M Deicher, G Grubel, R Keller, N Schulz, and H Skudlik, Appl Phys A48 (1989) 59-85

Chapter 1 General Introduction

1.1 Introduction

The existence of a wide range of electronic products from complex VLSI processor chips to novel sensor devices, and the constant developing and refining of the manufacturing techniques used, have been made possible, in part, through making use of the information provided by the continuing study of the properties of semiconductors, the materials from which these devices are made Semiconductors have become such a major part of the electronics industry because their properties can be greatly and precisely altered by controlling the introduction of impurities and imperfections in the material.

Chemical impurities, such as boron or phosphorous in substitutional sites in crystalline silicon or germanium, produce energy levels in the band gap of the crystal very close to the band edges and generally contribute extra charge carriers, electrons or holes. These are called shallow impurities and their role is primarily to control the conductivity level and type. Other impurities and various simple lattice defects and impurity-defect complexes can produce energy levels deep in the band gap and are referred to as deep centres. They act as carrier traps or recombination centres and their role is dependent on the application. For instance they are undesirable in devices such as solar cells where carriers must have long lifetimes On the other hand they are useful in fast switches where the carrier concentration must be reduced sharply on a short time scale. Deep centres are also used in making light-emitting diodes when the

recombination or carrier-capture energy is released as light

Shallow impurities and deep centres are usually of atomic or molecular dimensions and are more generally referred to as point defects Semiconductors are also known to contain defects which are of larger dimensions, such as dislocations, grain boundaries, stacking faults and precipitates These are called extended defects Although these defects sometimes affect the electrical properties of the semiconductor they generally have a more significant effect on the more macroscopic properties, such as tensile strength and elasticity Dislocations and precipitates have been shown to be efficient in gettering unwanted impurities from the areas of a wafer where devices are constructed. However, single crystals free of extended defects are generally desirable for device manufacturing applications [1] Thus all types of defects have both useful and detrimental features and the study of these defects in semiconductors has been an active field of scientific research since semiconductors emerged as technologically important materials

The work presented in this thesis is concerned with the photoluminescence characterisation of an indium-implantation damage related defect in silicon. This chapter aims to provide an introduction to defects in silicon, to the photoluminescence characterisation technique and to why an indium related defect was studied

1.2 The silicon crystal structure

A silicon crystal structure consists of a three dimensional array of silicon atoms covalently bonded in a tetrahedral arrangement Each silicon atom is bonded to its four nearest neighbours with all atoms sitting on a regular lattice site. The lattice structure is made up of two inter-penetrating face-centred cubic arrays which are based on the points (0,0,0) and (1/4,1/4,1/4) The crystal has highly directional valence bonds in <111> directions with every atom being at the centre of a tetrahedron with the four nearest neighbour atoms situated one at each vertex The conventional cubic cell of the silicon lattice is shown in Figure 1 1.

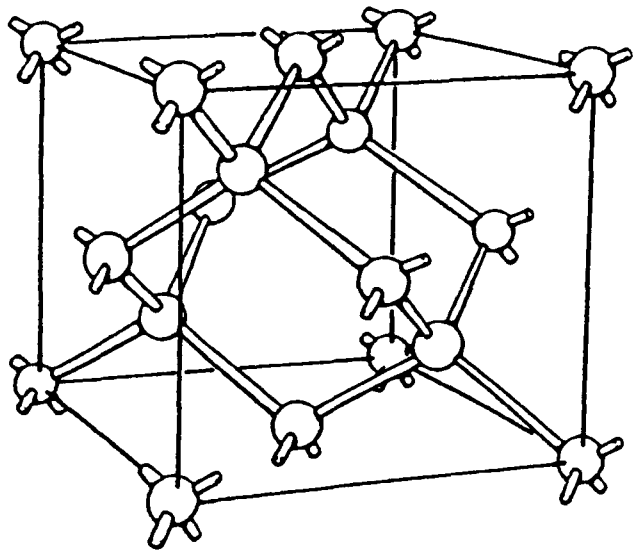

Figure 1.1 The conventional cubic cell of the silicon lattice

An idealised silicon crystal would have no defects or deviations from the periodicity of the lattice structure. Real crystals, however, always have some structural imperfections. These imperfections can be divided into two main types, point defects

and extended defects Point defects can be divided into two classes, intrinsic and extrinsic point defects Intrinsic point defects include vacancies and interstitials Vacancies are lattice sites which are missing an atom and interstitials are extra atoms which occupy positions in the crystal structure not on regular lattice sites Extrinsic point defects include impurity atoms in substitutional or interstitial lattice sites or complexes of intrinsic defects and impurity atoms. Point defects are usually of atomic or molecular dimensions and retain a high degree of symmetry

Extended defects include dislocations, which are misalignments of rows of atoms in the crystal; grain boundaries, which mark the interfaces between regions of different crystal orientation, stacking faults, which arise from an error in layer growth and precipitates which can be considered as aggregates of point defects which are so large that their symmetry properties have been lost.

As the work presented in this thesis is concerned with the characterisation of point defects associated with implantation damage in silicon, extended defects will not be dealt with in any more detail A schematic diagram of some simple point defects is shown in Figure 1.2

Impurities and defects are introduced into silicon, intentionally or unintentionally in a number of ways·

1. In the crystal growth process there are always some trace impurities such as carbon and oxygen present in the starting material;
2. Impurities can be intentionally added during the growth process to produce n-type or p-type material,
3. Impurities can diffuse in from the surface;
4 Defects are produced during ion implantation and by electron irradiation;

5 Transmutation doping by irradiating the host atoms with neutrons,

6 Quenching and heat treatments activate the formation of impurity-intrinsic defect complexes.

In device manufacturing, several of the above methods may be used at different stages of the manufacturing process, depending on the required effect The work presented here is concerned with the characterisation of a defect produced by the ion implantation method followed by annealing.

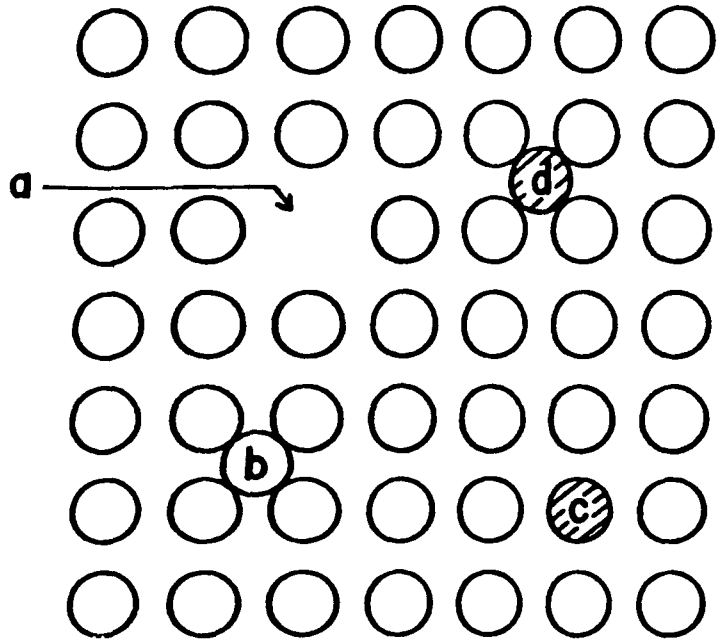

Figure 1 2 Simple point defects: (a) vacancy; (b) interstitial; (c) substitutional impurity; (d) interstitial impurity.

1.3 Photoluminescence characterisation

Photoluminescence (PL) spectroscopy is a very sensitive technique for investigating the optical properties of semiconductors and insulators Since the 1970's, when rapid advances began in the semiconductor industry and new detectors like the intrinsic germanium detectors were developed which extended the wavelength range and gave improved signal to noise ratios, the number of PL systems studied in silicon has greatly increased

The term photoluminescence refers to the luminescence which is produced when a material is excited with photons as opposed to carrier injection (electroluminescence) or accelerated electrons (cathodoluminescence). Photoluminescence detects an optical transition from an excited electronic state to a lower electronic state. The photoluminescence resulting from a transition is characteristic of either intrinsic transitions or transitions at impurities or defects in the material From the spectroscopic identification of the transition information about the electronic structure of the material and its defects can be inferred

1.3.1 Photoluminescence of silicon

Photoluminescence is usually generated in silicon by illuminating it with, for example, Ar or Kr laser light with photon energy greater than the band gap The energy gap between the valence and conduction bands in silicon is indirect, decreasing from 1 17 eV at low temperature to approximately 1.12 eV at room temperature This

indirect gap is located at k_m = 0 80 ± 0 05 of the zone boundary lattice vector along the <001> axes from k=0 A schematic diagram of the silicon band structure in the <100> direction is shown in Figure 1 3(a)

Photons with energy substantially greater than the band gap energy are strongly absorbed by electron excitation at constant wavevector The depth of penetration of, for instance, photons of 2.5 eV (Ar laser) at the 1/e intensity level is approximately 1μm [2]. For photon energies close to the band gap energy an electron can only be excited from the upper valence band at k=0 to the conduction band minimum at k_m if a phonon of wavevector $-k_m$ is created or one of k_m absorbed to conserve wavevector in the transition A diagram of the phonon dispersion curves for silicon, in the <100> direction, is shown in Figure 1.3(b). Some energy values of phonons with the same wavevector as the conduction band minimum, k_m, are [2,3]

$\hbar\omega$ = 18 4 ± 0 2 meV, transverse acoustic (TA) mode,

= 56 0 ± 1 meV, longitudinal optic (LO) mode,

= 58 0 ± 1 meV, transverse optic (TO) mode,

= 64.2 meV, zone-centre cut-off (O^{Γ})

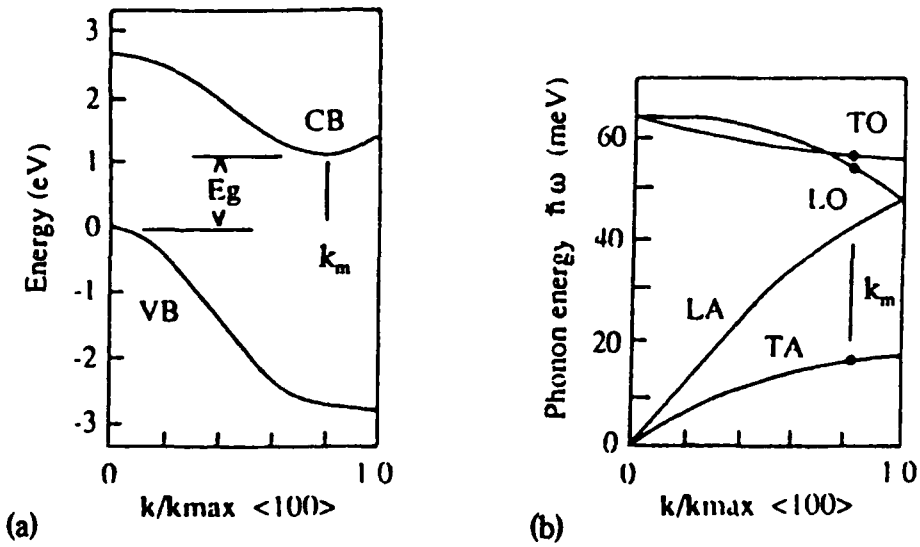

Figure 1 3 (a) The band structure of silicon in the <100> direction showing the valence band (VB), the conduction band (CB), the band gap (Eg) and the wavevector position of the conduction band minimum (k_m). (b) The phonon dispersion curves for silicon in the <100> direction. LO, LA, TO, TA are the longitudinal optic and acoustic and transverse optic and acoustic phonon modes respectively, k_m is the wavevector position of the conduction band minimum.

When silicon is excited at low temperature (T < 30 K) with photons having energy greater than the band gap electron-hole pairs are produced. These can recombine in a number of ways, as shown schematically in Figure 1 4, some radiative, giving rise to luminescence, and others non-radiative. The luminescence intensity associated with a particular path depends on the relative and absolute concentrations of various impurities and defects, the excitation density and the temperature, and involves capture cross-sections and branching ratios for radiative and non-radiative decay.

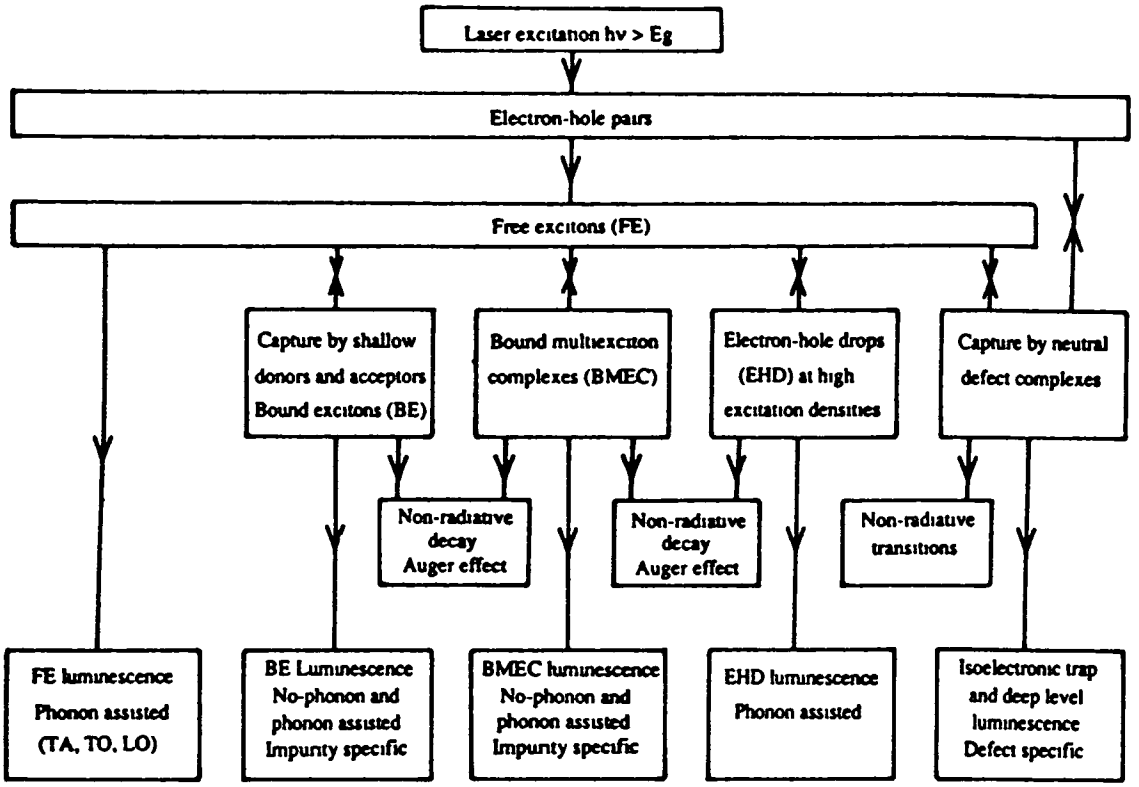

Figure 1.4 Luminescence decay processes stimulated by above band gap photoexcitation

At low temperatures and with low excitation densities the electron hole pairs form free excitons In high purity material where the number of defects and impurities that can trap excitons is low the free excitons recombine giving rise to luminescence. Because of the indirect band gap of silicon, phonons with the same wavevector as the conduction band minimum must be emitted with the free exciton luminescence to conserve wavevector or momentum ($\hbar k$) in the transition (left hand path in Figure 1.4). A photoluminescence spectrum of near intrinsic silicon is shown in Figure 1.5. The free exciton (FE) phonon assisted transitions are the dominant features. Luminescence associated with trace amounts of boron, phosphorous, aluminium and arsenic are labelled

B, P, Al, and As accordingly Features labelled NP are impurity related no-phonon transitions, while features labelled TA, TO and LO are transitions assisted by the emission of transverse acoustic, transverse optic and longitudinal optic phonons respectively

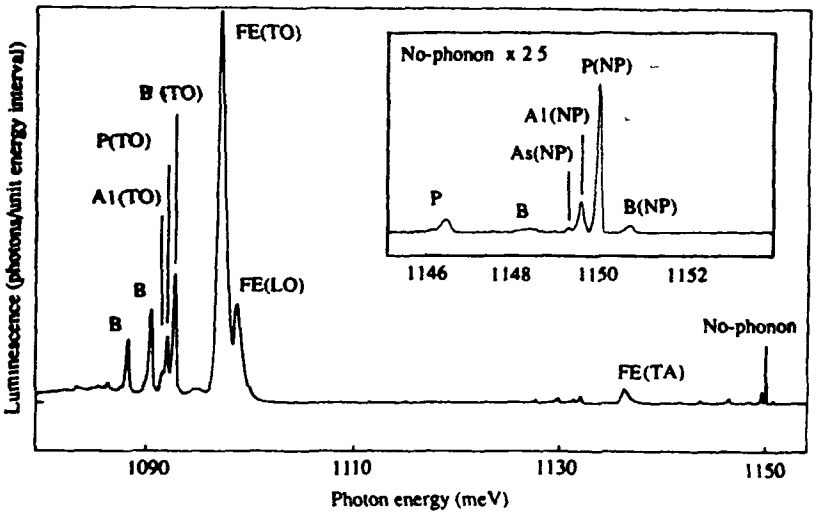

Figure 1 5 Photoluminescence spectrum of near intrinsic silicon Taken from [4].

When the concentration of exciton traps such as donor and acceptor impurities added to the material increases, the probability that the free excitons which diffuse through the material will be captured by these traps increases. Excitons trapped at shallow donors or acceptors are bound with a binding energy of a few meV depending on the impurity species (3 8 meV for B, 4.7 meV for P). These bound excitons recombine leading to impurity specific bound exciton luminescence. Bound exciton

recombination can occur with or without the emission of phonons The luminescence lines are sharp with photon energies given by

$$h\nu = Eg - Ex - Eb \ (-\hbar\omega)$$

where Eg is the energy gap, Ex is the exciton binding energy, Eb is the binding energy of the exciton to the donor or acceptor and $\hbar\omega$ is the energy of the phonon involved in the transition, if any.

Figure 1 6 shows a photoluminescence spectrum of a silicon sample doped with $3x10^{14}$ cm^{-3} P with negligible B, Al and As The dominant features are the phosphorous bound exciton no-phonon line and the TO phonon assisted line At increased excitation densities the donors and acceptors bind more than one exciton, and additional lines appear associated with the recombination of two (α_2), three (α_3) and four (α_4) excitons (the bound multi-exciton complexes (BMEC) path in Figure 1.4). At very high excitation densities (eg 3 MWm^{-2}) the electrons cannot de-excite fast enough through exciton recombination and the densities of electrons and holes in the conduction band minimum and valence band maximum increases. The electrons and holes condense into a plasma, referred to as an electron-hole liquid or electron-hole drops The dominant electron hole recombination process is non-radiative but a weak recombination luminescence produces a very broad band on the low energy side of the free exciton structure [9]

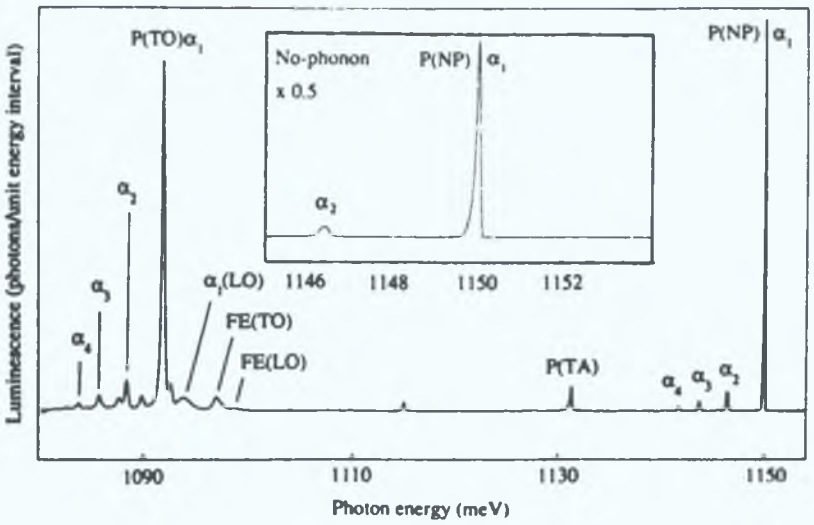

Figure 1.6 Photoluminescence spectrum from a silicon sample doped with $3x10^{14}cm^{-3}$ P with negligible B, Al and As. Taken from [4].

The extreme right hand path in Figure 1.4, recombination luminescence at isoelectronic traps, is responsible for a large number of luminescence systems in silicon. Isoelectronic means the trap is electrically neutral with respect to the silicon lattice. Substitutional impurity atoms with the same number of valence electrons as silicon e.g. carbon or germanium, are isoelectronic defects. However, exciton recombination at this type of isoelectronic point defect has not been reported for silicon. The isoelectronic centres which have been identified in silicon are molecular type defects consisting of impurity-impurity and impurity-intrinsic defect complexes produced by contamination with transition elements, radiation damage and/or heat treatments. Hopfield et al. [5] proposed a model for such defects: a short range force, such as a local strain field about the defect site, tightly binds an electron or hole. This charged particle can then capture

by Coulombic attraction a hole or electron This electron hole pair is referred to as an isoelectronically bound exciton (IBE) Because of the asymmetry in carrier binding, the centre can act as an acceptor if the electron is the tightly bound particle or as a donor if the hole is tightly bound. These are normally referred to as isoelectronic acceptors or isoelectronic donors. The Hopfield model was confirmed by Cohen and Sturge [6] in 1977 for near neighbour nitrogen pairs in GaP. Weber et al [8] in 1979 were one of the first to identify isoelectronic centres in silicon and since then many more have been reported [2]

1.3.2 PL intensity temperature dependence

The temperature dependence of the photoluminescence intensity from many optical centres in silicon is often very similar At higher temperatures $T \geq 30$ K the intensity decreases rapidly and at lower temperatures $0 < T < 25$ K the luminescence intensity often increases, with the increase being sample dependent The decrease at higher temperatures may result from either a thermal equilibrium existing between the excitons captured at the optical centre and free excitons or the free excitons thermally dissociate before they can be captured by the centre The increase in the lower temperature regime arises from the competition for capturing the excitons between the optical centre and shallower traps. As the temperature increases excitons freed from shallow traps become available for capture by other deeper traps such as optical centres, as a result the luminescence from these centres increases The temperature dependence of the no-phonon lines of two deep centre defects is shown in Figure 1 7. The 767

meV line is called the P-line and the 1018 meV line is called the W-line Both are produced by irradiation damage and annealing It can be seen that the intensity of each line increases with increasing temperature, up to approximately 30 K, after that the intensity decreases This behaviour is typical of these types of defects [2]

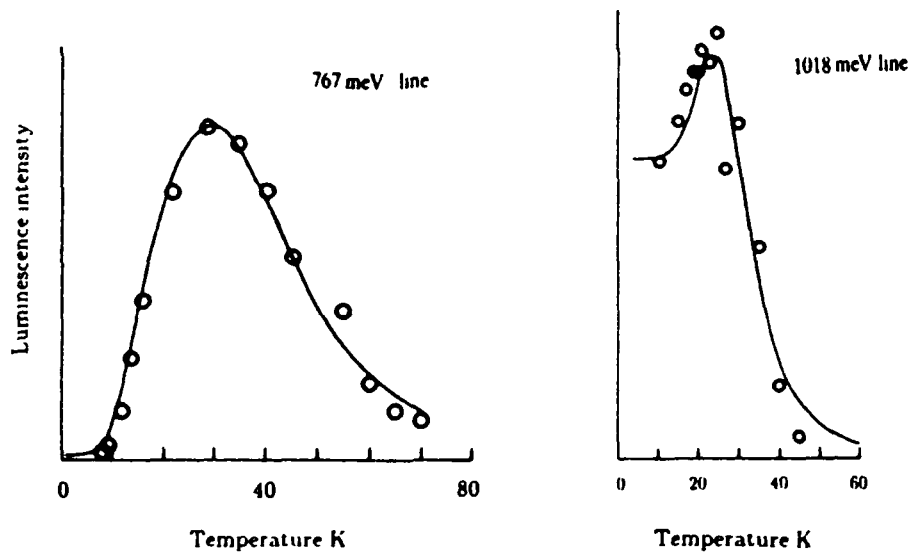

Figure 1 7 Temperature dependence of no-phonon lines of two deep centres. Taken from [2].

1.3.3 Identification of defect complexes

An important factor in the characterisation of defects using photoluminescence is identifying the specific spectral features with the defect responsible In the case of donor and acceptor bound exciton luminescence this is relatively straight forward as the intentional doping with various donors and acceptors is a reasonably well controlled

process For other defects, particularly defect complexes formed unintentionally by, for instance, implantation damage or during thermal treatments, it is not as easy to identify the constituents of the defect If it is suspected that a particular impurity is involved in the defect intentional doping with known ratios of different isotopes of that impurity can help to unambiguously identify it as a constituent. For example, the photoluminescence spectrum of a radiation-damage-produced defect in Czochalski (CZ) grown silicon is shown in Figure 1 8(a). This is the now well known C-line defect. Figure 1.8(b) shows the no-phonon line in an irradiation damaged CZ sample doped with both ^{12}C and ^{13}C The no-phonon line split into two components in roughly the same ratio as the carbon isotopes, which suggested that the defect contained one carbon atom. Samples doped with both the oxygen isotopes ^{16}O and ^{18}O showed no splitting for the no-phonon line but the local mode features L1 and L2 did show some isotope splitting, Figure 1 8(c),(d) This indicated that one oxygen atom was also involved in the defect.

Isotope substitution can provide information about the impurities involved in the defect. Other techniques, however, are required to establish the structural arrangement of the constituents of the defect within the silicon lattice To this end, uniaxial stress spectroscopy is one technique which is commonly used to provide information about the symmetry of the defect

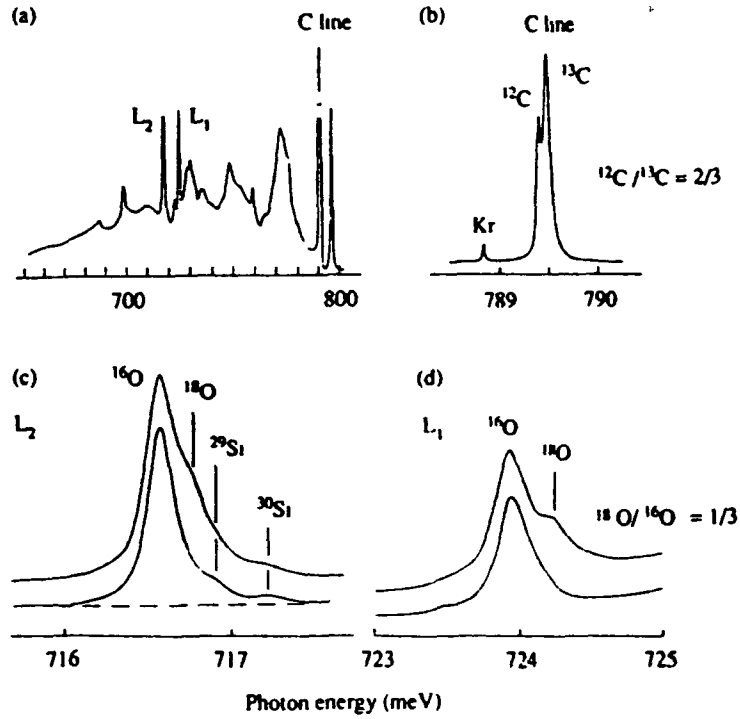

Figure 1.8 Isotopes splitting of the no-phonon line and the local mode lines of the C-line luminescence system Taken from [9].

1.3.4 Uniaxial stress spectroscopy

The very narrow no-phonon luminescence line associated with the recombination of excitons at an optical centre in silicon make it possible to measure directly small shifts and splittings of the line as a result of an applied uniaxial stress This technique has been widely used to determine the symmetry class of the optical centre and the symmetry properties of the electronic states involved in the transition. The splitting in

the line arises from the removal of either orientational degeneracy, orientational and electronic degeneracy or purely electronic degeneracy

The silicon lattice has cubic symmetry A regular defect centre in the lattice structure can be characterised by its point symmetry group Usually the symmetry elements of the defect coincide with symmetery elements of the crystal and the defect point group is a subgroup of the cubic group of the crystal The possible subgroups of the cubic group can be classified into eight symmetry systems. Six of these are shown schematically in Figure 1 9 The other two systems are cubic, whose symmetry axes must coincide with the lattice axes, and triclinic, for which there are no restrictions on defect orientation. Each of the eight systems except the cubic class have a number of equivalent orientations in the unstressed crystal For instance, a trigonal centre has one three fold axis which can align along one of the four equivalent three fold axes of the silicon crystal ((111) directions) The C_4 axis of a tetragonal centre must lie along one of the three equivalent four fold axes ((100) directions) of the crystal Under uniaxial stress the crystal structure is deformed and equivalent orientations in the unstressed crystal are no longer equivalent For each inequivalent orientation there may be a separate transition energy due to the effects of strain on the energies of the initial and final states

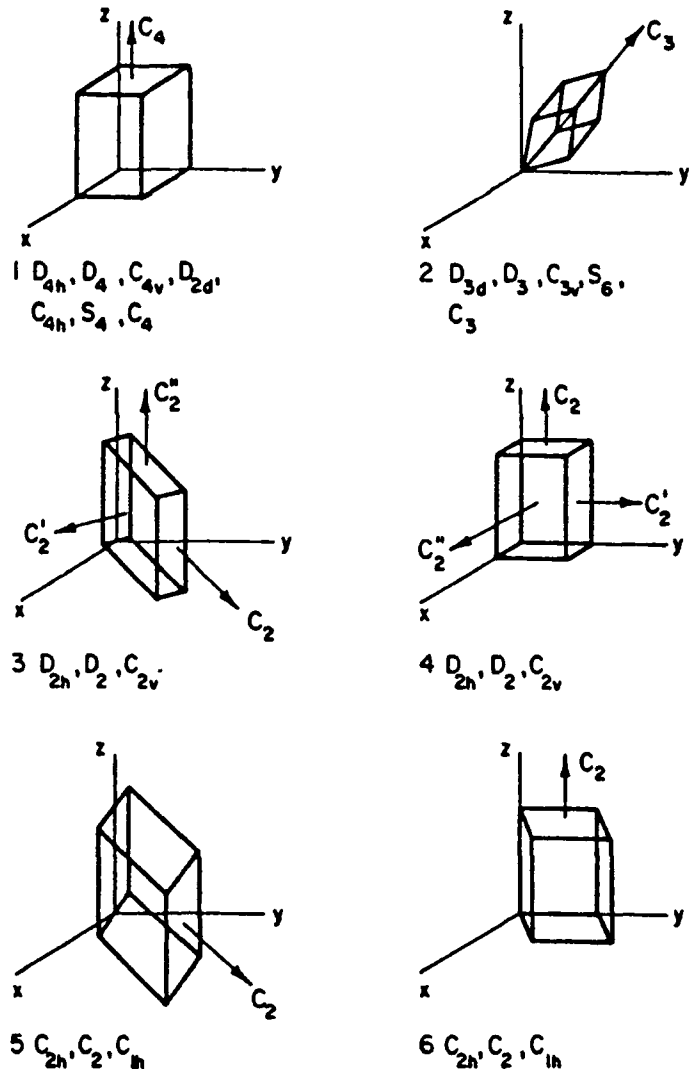

Figure 1.9 Schematic representation of six of the eight possible symmetry systems for defects in cubic crystals, with the possible point groups for each system: (1) tetragonal, (2) trigonal, (3) rhombic I, (4) rhombic II, (5) monoclinic I, and (6) monoclinic II.

The quantities of interest in the splitting of the no-phonon line at the defect centres are the number of split components and the intensity, polarisation and energy shift of each component under uniaxial stress applied in the main symmetry directions of the crystal. A list of all the possible transitions at all the possible defect centres in cubic crystals, with the number of stress split components for uniaxial stress applied along the three major crystallographic directions, is given in Table 1.1.

Type of centre and electronic transition	Number of stress-split components under relevant stress direction <100>	<111>	<110>
1 Tetragonal (A→A)	2	1	2*
2 Trigonal (A→A)	1	2	2
3 Orthorhombic I (A→A)	2	2	3
4 Orthorhombic II (A→A)	3	1	3
5 Monoclinic I (A→A)	2	3	4
6 Monoclinic II (A→A)	3	2	4
7 Triclinic (A→A)	3	4	6
8 Tetragonal (A→E)	3	2	4*
9 Tetragonal (E→E)	3	2	4*
10 Trigonal (A→E)	2	3	4*
11. Trigonal (E→E)	4	5	8
12 Tetrahedral ($T_1 \rightarrow T_2$)	3	4	6
13. Tetrahedral ($A_1 \rightarrow T_1$, $A_2 \rightarrow T_2$)	2	2	3
14. Tetrahedral ($E \rightarrow T_1$, $E \rightarrow T_2$)	3	2	5
15 Tetrahedral ($T_1 \rightarrow T_1$, $T_2 \rightarrow T_2$)	3	3	6
16 Tetrahedral ($\Gamma_8 \rightarrow \Gamma_8$)	4	4	4
17. Tetrahedral ($\Gamma_6 \rightarrow \Gamma_8$, $\Gamma_7 \rightarrow \Gamma_8$)	2	2	2

Table 1 1 Number of components in the splitting patterns of all transitions possible at centres within the silicon lattice * indicates that the number of components observable for <110> stress is not mdependent of viewing direction In transition numbers 1 to 11 no distinction is made for transitions between A_1, A_2 and B states, as the number of stress-split components is the same in each case.

The first group are transitions involving non-degenerate electronic levels where only the orientational degeneracy of the defects is removed The second group corresponds to transitions at trigonal and tetragonal centres where both orientational and electronic degeneracy are removed and the third group to transitions at tetrahedral centres where only electronic degeneracy is removed.

The derivation of the number of stress split components, the intensity and polarisation, and the shift rate parameters for each component for these three categories involves the application of group theory and first-order perturbation theory Detailed treatments of the derivations have been given in several papers by Kaplyanskii [10,11], Hughes and Runciman [12] and Mohammed et al [13] The results for the most common types of symmetry systems are given in tabular form in Tables 1 2 and 1.3 and by schematic representation in Figure 1.10

Type of centre	Stress direction		
	<100>	<111>	<110>
1 Tetragonal	A_1 A_2	1/3 (A_1 + A_2)	1/2 (A_1 + A_2) A_2
2 Trigonal	A_1	A_1 + 2 A_2 A_1 - 2/3 A_2	A_1 + A_2 A_1 - A_2
3 Rhombic I	A_2 A_1	1/3 (A_1 + 2 A_2 + 2 A_3) 1/3 (A_1 + 2 A_2 - 2 A_3)	A_2 + A_3 1/2 (A_1 + A_2) A_2 - A_3
4 Rhombic II	A_1 A_2	1/3 (A_1 + A_2 + A_3)	1/2 (A_1 + A_2) 1/2 (A_1 + A_3) 1/2 (A_2 + A_3)
5 Monoclinic I	A_2 A_1	1/3 (A_1 + 2 A_2 + 2 A_3) 1/3 (A_1 + 2 A_2 - 2 A_3 - 4 A_4) 1/3 (A_1 + 2 A_2 - 2 A_3 + 4 A_4)	A_2 + A_3 1/2 (A_1 + A_2 - 2 A_4) 1/2 (A_1 + A_2 + 2 A_4) A_2 - A_3
6 Monoclinic II	A_1 A_2 A_3	1/3 (A_1 + A_2 + A_3 + 2 A_4) 1/3 (A_1 + A_2 + A_3 - 2 A_4)	1/2 (A_1 + A_2) 1/2 (A_1 + A_3) 1/2 (A_2 + A_3 + 2 A_4) 1/2 (A_2 + A_3 - 2 A_4)
7 Triclinic	A_1 A_2 A_3	1/3 (A_1 + A_2 + A_3 + 2 A_4 + 2 A_5 + 2 A_6) 1/3 (A_1 + A_2 + A_3 - 2 A_4 + 2 A_5 - 2 A_6) 1/3 (A_1 + A_2 + A_3 - 2 A_4 - 2 A_5 + 2 A_6) 1/3 (A_1 + A_2 + A_3 + 2 A_4 - 2 A_5 - 2 A_6)	1/2 (A_1 + A_2 + 2 A_4) 1/2 (A_1 + A_2 - 2 A_4) 1/2 (A_1 + A_3 + 2 A_6) 1/2 (A_1 + A_2 - 2 A_6) 1/2 (A_2 + A_3 + 2 A_5) 1/2 (A_2 + A_3 - 2 A_5)

Table 1 2 Stress shifts for centres with orientational degeneracy only. The expressions give the energy shift for each component, the parameters A_i relate the perturbing potential to the stress tensor. The notation is that of Kaplyanskii [10].

Type of centre	Stress direction		
	<100>	<111>	<110>
Tetragonal (A ↔ E) or (E ↔ E)	α β	1/3 ($\alpha + \beta + \gamma - \delta$) 1/3 ($\alpha + \beta + \gamma + \delta$)	1/2 ($\alpha + \beta$) 1/2 ($\beta + \gamma - \delta$) 1/2 ($\alpha + \gamma$) 1/2 ($\beta + \gamma + \delta$)
Trigonal (A ↔ E)	$\alpha + \beta$ $\alpha - \beta$	$\alpha - 2\,\delta$ $\alpha - 4/3\,\gamma + 2/3\,\delta$ $\alpha + 4/3\,\gamma + 2/3\,\delta$	$\alpha - \beta/2 - \gamma - \delta$ $\alpha + \beta/2 + \gamma - \delta$ $\alpha - \beta/2 - \gamma + \delta$ $\alpha + \beta/2 - \gamma + \delta$

Table 1 3 Stress shifts for centres with both electronic and orientational degeneracy The expressions give the energy shifts for the stress-split components in each direction Here α, β, γ and δ are stress coefficients which relate the energy shift to the applied stress tensors The notation is that of Fitchen [45].

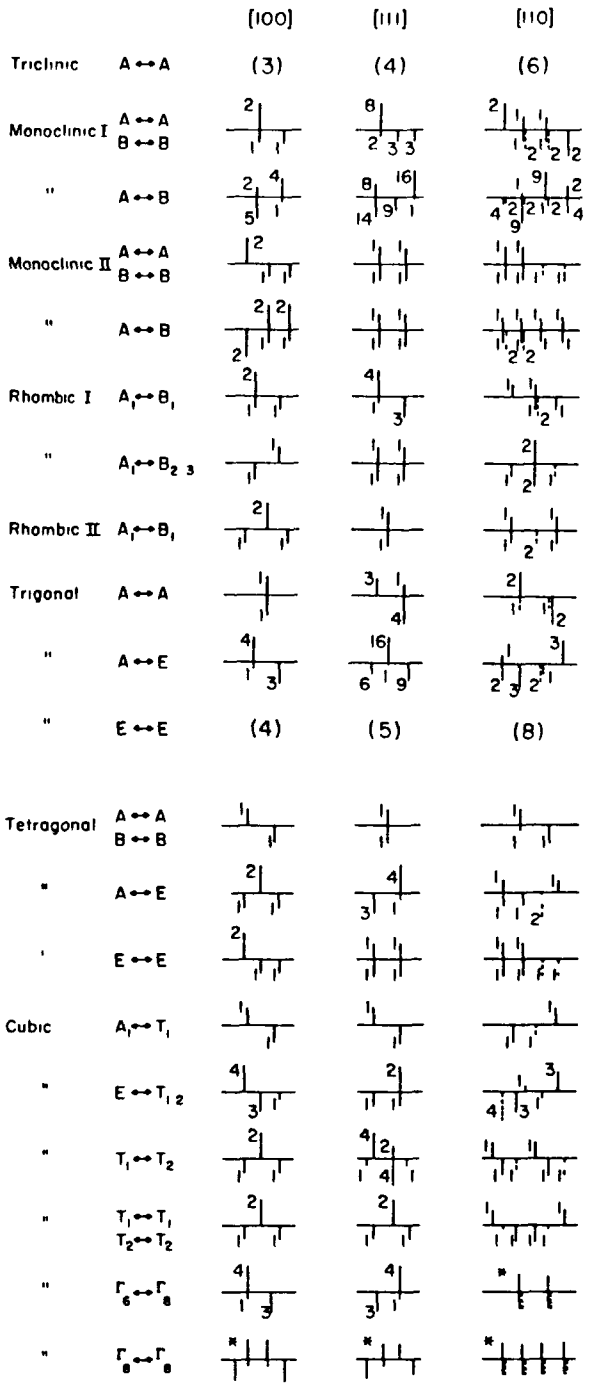

Figure 1 10 Schematic splittings of no-phonon lines under uniaxial stress for various transitions at centres belonging to the eight possible symmetry systems for cubic crystals The spacing of the split lines is arbitrary and the relative intensities are indicated by the small numerals The vertical lines above the horizontal lines are polarised parallel to the stress direction, and those below perpendicular to it. For a [110] stress, there are two inequivalent perpendicular polarisations, [1$\bar{1}$0] (——) and [001] ( ) The asterisk indicates that the intensity ratios are not unique Taken from [45].

The first stage in identifying the transition and the defect symmetry in practice is to compare the number of experimentally found stress split components with the number predicted by theory (listed in Table 1 1 or Figure 1 10) This reduces the number of possibilities and in some cases can be enough to positively identify the transition and defect symmetry The next stage is to measure the shift rates, relative intensities and polarisation of all the stress split components The intensity and polarisation data can help to identify the stress split components with the relevant theoretically derived equations involving the stress shift parameters (Table 1 2, 1.3). A set of simultaneous equations involving the shift parameters and the experimentally measured shift rates are then solved to find values for the parameters The defect is characterised by its symmetry group, the symmetry properties of the electronic levels involved and the values found for the shift parameters

1.4 Objectives

Many materials characterisation techniques have been developed over the years to study, from different perspectives, the various properties of semiconductors. For instance deep level transient spectroscopy (DLTS) and Hall effect measurements are used to study the electrical properties of materials while photoluminescence (PL) and absorption spectroscopy are used to study the optical properties In recent years the perturbed angular correlation spectroscopy (PAC) technique, which was mainly used for the study of metals, has been used to study defect production due to ion implantation in semiconductors and crystal regrowth during annealing [14].

The PAC technique uses the hyperfine interaction between a radioactive probe and its environment to provide information on defect structure and annealing properties The technique tells little about the electronic properties of the defect PL on the other hand detects optical transitions from an excited electronic state to a lower electronic state thus providing direct information of electronic levels. The symmetry of the defect can also be deduced by combining PL and perturbation techniques such as uniaxial stress and Zeeman measurements.

The aim of the work presented in this thesis was to show that PL provides a complementary technique to PAC and other nuclear techniques used for semiconductor characterisation and to investigate the use of radioactive isotopes to identify the constituents of defects observed in photoluminescence The reason why a PL study of indium implanted silicon was carried out was because the radioactive indium isotope, indium-111, is commonly used as a suitable radioactive probe, in silicon, necessary for performing PAC spectroscopy To compare the PL and PAC techniques a PL study was made of indium implanted silicon and the results were compared with results of PAC studies of indium implanted silicon previously reported in the literature

Chapter 2 A review of indium doped silicon

2.1 Photoluminescence of Si:In

Impurity related luminescence from silicon was first reported by Haynes [15]. Dean et al. [16], in a comprehensive study of luminescence associated with various group V donors and group III acceptors in silicon, observed and identified luminescence arising from the radiative recombination of excitons bound to the deep acceptor indium. Indium acceptor bound exciton no-phonon and TO-phonon assisted peaks were observed at energies of 1.1413 eV and 1.0835 eV, respectively. More accurate values for these transition energies were obtained by Vouk and Lightowlers [7] in 1977.

Some luminescence spectra observed by Vouk and Lightowlers for indium doped silicon at various sample temperatures are shown in Figure 2.1 [7]. They were able to resolve and identify the doublet splitting of the bound exciton no-phonon (BE(NP)) and TO-phonon assisted (BE(TO)) peaks, only seen previously in absorption [17] and also to identify bound exciton LO, TA and TO+O^{Γ} phonon assisted peaks. The energies of the observed indium acceptor associated lines are given in Table 2.1 [7].

The origin of the lines labelled U2 - U5 in Figure 2.1 was unknown. The intensity of the lines was sample dependent and they were thought to be due to some unknown defect or impurity introduced during crystal growth. Mitchard et al [18] measured the luminescent lifetimes of the lines U2 and U3, which they labelled P and R and a third line, Q. They found that the lines had much longer decay times than those of excitons bound to neutral donor or neutral acceptor impurities and concluded

that they must arise from excitons bound to isoelectronic complexes containing indium and some other unidentified constituents. They suggested that the three lines were associated with transitions at three distinct binding centres. Subsequent studies however showed that the three lines arise from transitions involving various initial and final states of the same centre [19].

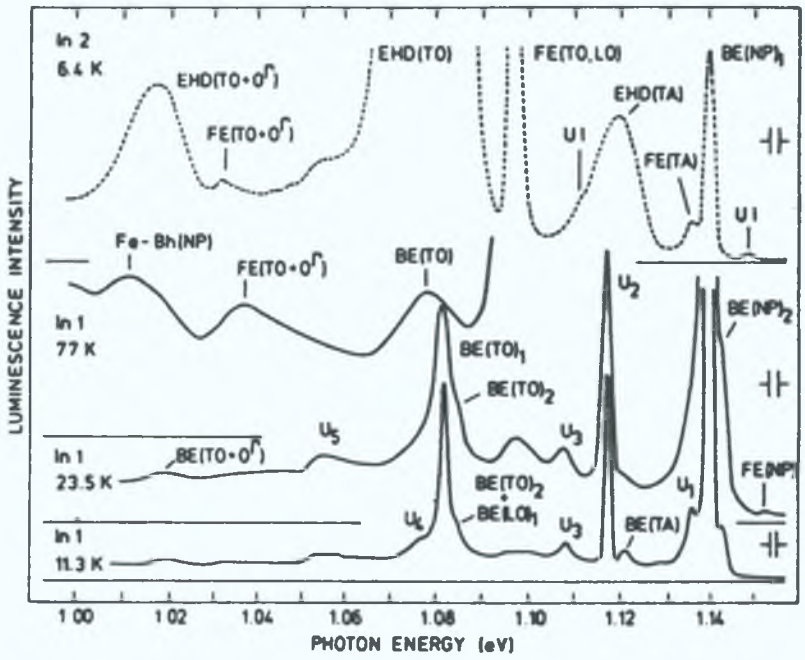

Figure 2.1 Luminescence spectra obtained from indium doped silicon at various sample temperatures. Taken from [7].

Line	Peak energy (eV)
$BE(NP)_2$	1.14386 ± 0.00012
$BE(NP)_1$	1.14076 ± 0.00006
$BE(TA)_{1,2}$	1.1216 ± 0.0002
$BE(LO)_1 + BE(TO)_2$	1.08455 ± 0.00031
$BE(TO)_1$	1.08263 ± 0.00012
$BE(TO + O^{\Gamma})$	1.0197 ± 0.0012

Table 2.1 Energies of the In-associated luminescence lines at 11.3 K [7].

Detailed studies of the properties of this indium related isoelectronic centre were made easier by the independent discovery by Thewalt et al [19] and Weber et al [20] of a rapid thermal quenching technique which greatly enhances the intensity of the PQR series of lines. A luminescence spectrum obtained from quenched indium doped silicon is shown in Figure 2 2 [19]

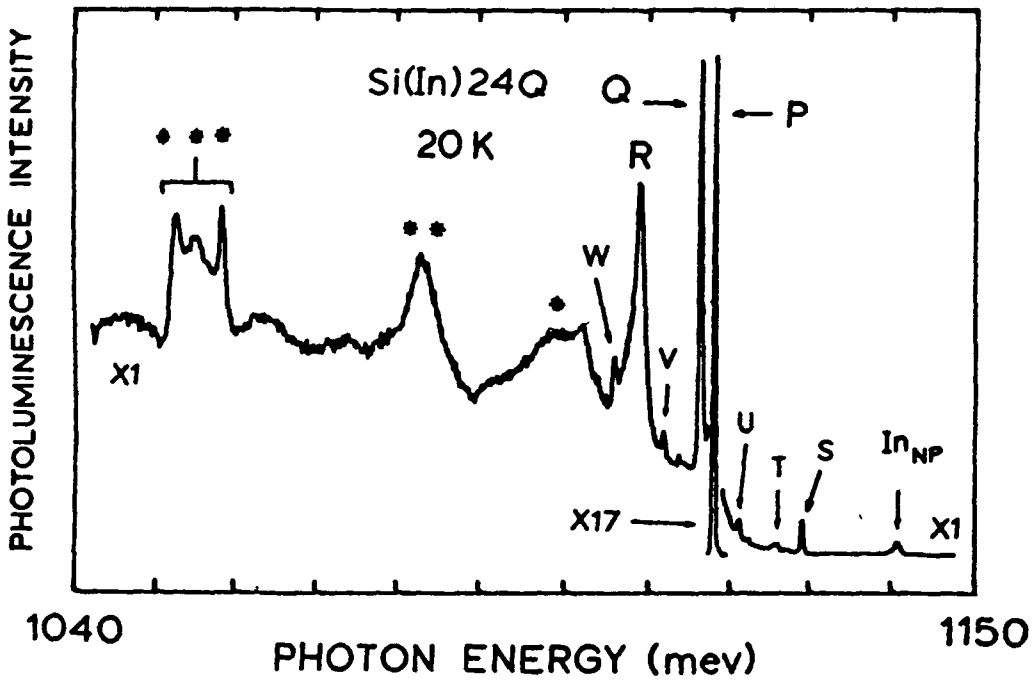

Figure 2 2 Photoluminescence spectrum of quenched In-doped silicon [19].

The PQR system has been one of the most widely investigated of any such complex in silicon. Much is now known about the spectroscopic nature of the complex Photoluminescence excitation (PLE) spectra taken by Wagner and Sauer [21] identified the strongest lines of the system as a no-phonon line and its Stokes side-band. In PL and PLE spectroscopy studies of the system under uniaxial stress and magnetic

perturbations Watkins and Thewalt [22,23] investigated the structure of the electronic states of the system The defect symmetry was unambiguously determined to be C_{2v} [23] From studies of the transient behaviour of the system, in comparison with a similar system observed in quenched thallium doped silicon, Watkins et al [24] concluded that the centre can exist in one of two configurations, with the interchange between the two configurations being thermally activated.

The identification of the constituents which render the In-related defect isoelectronic, however, remains unknown. Suggestions have included iron [20], phosphorus [25], hydrogen [19], carbon [26] and oxygen [27] None of the evidence has been conclusive. Brown and Bradfield [28] saw some correlation between the intensity of the PQR system and the presence of oxygen during the quenching treatment but they proposed oxygen as a catalyst for the formation of the defect and not as a constituent of the defect.

Conventional bulk doped or diffusion doped silicon and implantation doped silicon have been used in the investigation of the PQR system. In most cases the thermal quench treatment was used to enhance the PQR system intensity. In an investigation of the effects of thermal treatments and atomic H on the PL from indium implanted silicon Thewalt et al [29] annealed samples in the temperature range up to 300°C and at 1000°C with slow and fast quenches to room temperature. No PL data were presented for samples annealed in the temperature range between 300°C and 1000°C, which is the region with which we are concerned in this study

2.2 Radioactive indium-111 as a probe for PAC

In PL studies of silicon, indium impurities can be categorised as among the less widely studied - only two point defect associated PL spectra are known to involve In There exists another analytical technique, however, for which indium is the single most important impurity element - this technique is perturbed angular correlation spectroscopy (PAC) [30] The PAC technique provides information at a microscopic level about the environment of a radioactive probe by using the products of the radioactive decay process to monitor the hyperfine interaction between the probe and its surroundings. The radioactive indium isotope indium-111 is the most common of a number of suitable isotopes used

One of the first applications of the technique to the study of semiconductors was in 1977 when Kaufmann et al [31] implanted radioactive ^{111}In into Si in order to study the annealing behaviour of defects in the lattice region surrounding the implanted probe atoms These first attempts at applying the technique to semiconductors however were unsuccessful. It was not until the mid 1980s that conclusive results began to emerge. A review of the application of the PAC technique to the study of indium defect complexes in silicon was given by Wichert et al [14]. The application of the technique to the study of III-V semiconductors was discussed by Soares et al [32] and to II-VI semiconductors by Austin et al. [33].

A list of some of the known In-defect complexes in silicon is given in Table 2.2. The characteristic frequency given for each defect is specific to that defect and can be used to identify the defect in subsequent studies. The first three defects labelled In-De1 to In-De3 were complexes formed during the annealing of the radiation damage

produced by the implantation process. The complexes involved indium and some intrinsic lattice defects such as vacancies, interstitial atoms and/or common impurities found in silicon such as carbon and oxygen The formation and breaking of the defect complexes as observed during the annealing of the implantation damage are shown in Figure 2 3 [14]

The defects labelled In-X were defect complexes involving indium and some unknown constituent which were observed in silicon after a chemo-mechanical polishing treatment Using the characteristic frequency to identify the defect the X constituent was later shown to be copper [34].

Complex	Characteristic frequency (MHz)	
	78 K	295 K
In-De1		28
In-De2		142
In-De3	451	448
In-P1	182	179
In-As1	231	229
In-As2	240	238
In-Sb1	275	271
In-H1	360	349
In-H2	480	463
In-H3	270	
In-Li1	172	172
In-Li2	260	231
In-Li3	323	
In-X1	327	
In-X2	334	
In-X3	408	

Table 2.2 Some defect complexes in Si, observed by PAC [14]

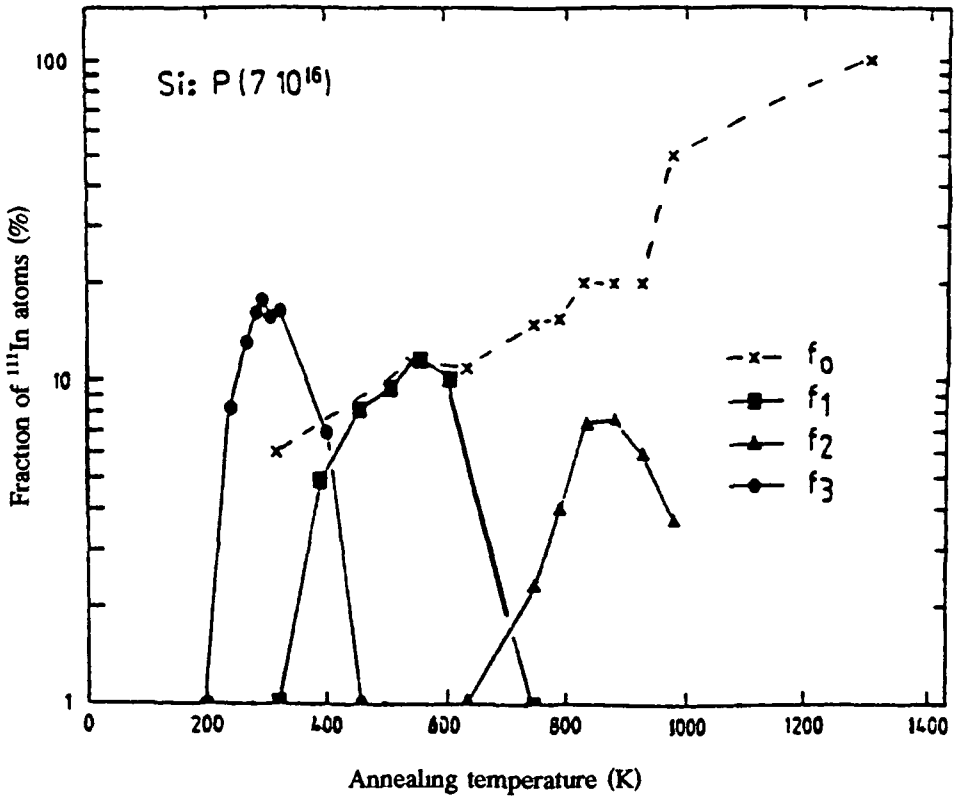

Figure 2 3 Fractions of In atoms in defect free or almost free sites (f_0) and in defect complexes In-De3 (f_3), In-De1 (f_1) and In-De2 (f_2) observed during isochronal annealing (10 min) of particle irradiated Si [14].

The In-H complexes listed in Table 2.2 were observed in investigations of the passivation of acceptors in silicon by atomic hydrogen [35]. Some PAC spectra showing the formation of the In-H complexes are shown in Figure 2.4(a),(b),(c) [14]. Figure 2.4(a) shows some typical PAC spectra; Figure 2 4(b) shows the Fourier Transforms of the PAC spectra identifying the characteristic frequencies of the defect complexes and Figure 2.4(c) shows the dependence of the populations of two types of In-H complexes on sample temperature

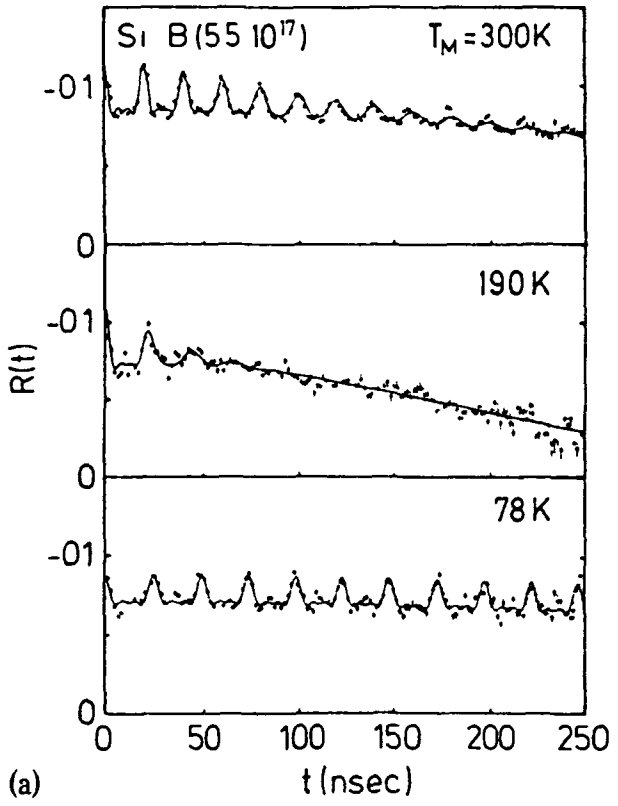

PAC spectra of ^{111}In in Si B (5.5×10^{17}) showing the formation of In-H1 at 300 K of In-H3 at 78 K and the transition between the two types of In-H complexes at 190 K which is accompanied by a pronounced dynamic relaxation process (note the damping of the oscillations)

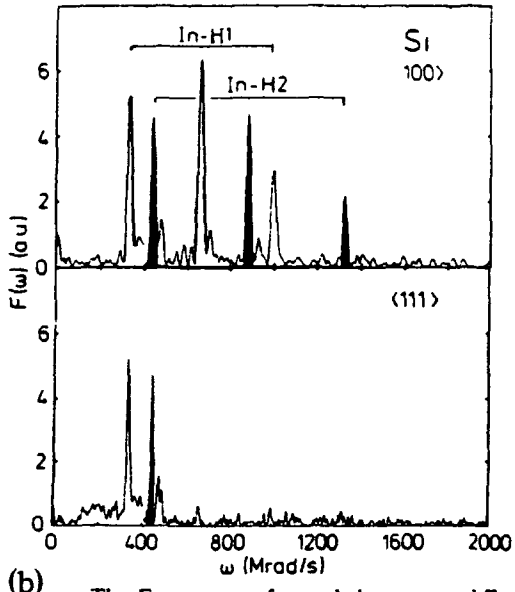

The Fourier transforms belonging to different orientations of the γ detectors with respect to the Si lattice show the $\langle 111 \rangle$ orientations of the complexes In-H1 and In-H2

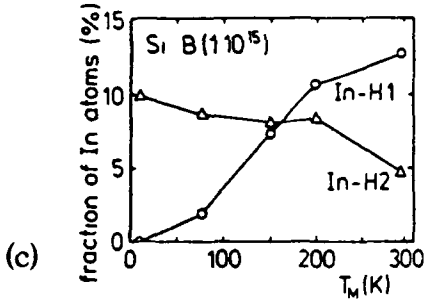

Influence of sample temperature on the populations of two types of In-H pairs

Figure 2.4 Some typical PAC spectra Taken from [14].

The PAC results for these indium related defect complexes can also provide information on the number of complexes formed, from which the activation energies of complex formation and breaking can be obtained

In addition to the study of specific properties of particular defect complexes the PAC technique has been used in a wider context. Recent studies of indium implanted silicon have investigated implantation damage annealing and the epitaxial regrowth of the silicon crystal, indium diffusion and the effect of silicon pre-amorphisation on the lattice location of the implanted indium atoms [36,37]

2.3 Correlation of PL and PAC

Perturbed angular correlation spectroscopy results have shown that the technique can provide information about implantation damage annealing, impurity diffusion processes, donor-acceptor pair formation, acceptor passivation, and the formation, dissociation, and geometric structure of defect complexes However, detailed information about the electronic structure of the defect complexes, which is important in the characterisation of opto-electronic materials, is not provided PL spectroscopy can supply information directly about the electronic levels of defects. It would be useful, for a more complete characterisation of the defects observed by PAC, to be able to correlate PAC results with PL results. Nobody has yet presented a study combining the two techniques The work presented in this thesis is a PL study of indium implanted silicon in an attempt to find some indium related complexes which could be identified with some of the indium complexes observed in PAC studies.

Chapter 3 Experimental details

3.1 Introduction

In a photoluminescence study there are usually a number of different experiments performed, such as annealing, temperature dependence, uniaxial stress and Zeeman measurements. The procedures used for preparing samples for these different PL experiments, the standard PL experimental apparatus and the arrangement used for uniaxial stress measurements are described below.

3.2 Sample preparation

The samples used for the preliminary experiments and the series of annealing experiments were cleaved from standard Czochralski-grown single crystal silicon wafers which were implanted with ^{115}In to a dose of 10^{14} cm^{-2} with an implantation energy of 150 keV Samples were taken from wafers of both p-type and n-type conductivities and of (111) and (100) orientations. The uniaxial stress experiments were performed on three samples cut from a boule of silicon into rectangular slabs of dimensions 11 mm x 4 mm x 2 mm in such a way that their long axes were oriented along one of the major cubic crystallographic directions <001>, <110>, <111>. These samples were also implanted with indium to the same dose and energy as the silicon wafers All samples were lightly doped, typically to a carrier concentration of 10^{14} cm^{-3}.

The oriented samples were etched, before implantation, in a 10 1 solution of HNO_3:HF to remove any surface damage which might have caused the samples to fracture when stress was applied All the samples were chemically cleaned before they were annealed, using a standard cleaning procedure (see Appendix A)

The samples were annealed in flowing nitrogen or helium gas in a conventional furnace After annealing the samples were allowed to cool slowly to room temperature

3.3 Experimental apparatus

A schematic diagram of a standard photoluminescence spectroscopy system is shown in Figure 3 1 An Oxford Instruments CF1204 continuous flow cryostat with liquid helium as the coolant was used in conjunction with an ITC4 temperature controller to allow the sample temperature to be maintained at any required temperature between 4 2 K and 300 K The samples were strapped to a sample holder with PTFE tape and positioned along the optical axis in the sample space of the cryostat.

The luminescence excitation was provided by the 514 5 nm line of an argon ion laser. Typical laser output power was 150 to 180 mW onto a sample area of approximately 3 mm diameter.

Photoluminescence, collected at an angle normal to the incidence excitation, was dispersed by a Spex 1704 one metre focal length Czerny-Turner spectrometer fitted with a 600 gr/mm grating blazed at 1.25 μm and detected by a North Coast EO-817 liquid nitrogen cooled germanium detector. The spectral range of this detector was 0.8 μm to 1 8 μm, with a peak in sensitivity at approximately 1 2 μm. The spectral range of

interest in the work presented in this thesis was approximately 1 1 μm to 1 3 μm The spectra recorded were not corrected for the overall response of the system since the response is approximately uniform across the range of interest.

The spectrometer grating drive was controlled by a computer and the output from the germanium detector after appropriate signal conditioning was fed back to the computer, making spectral acquisition fully computerised

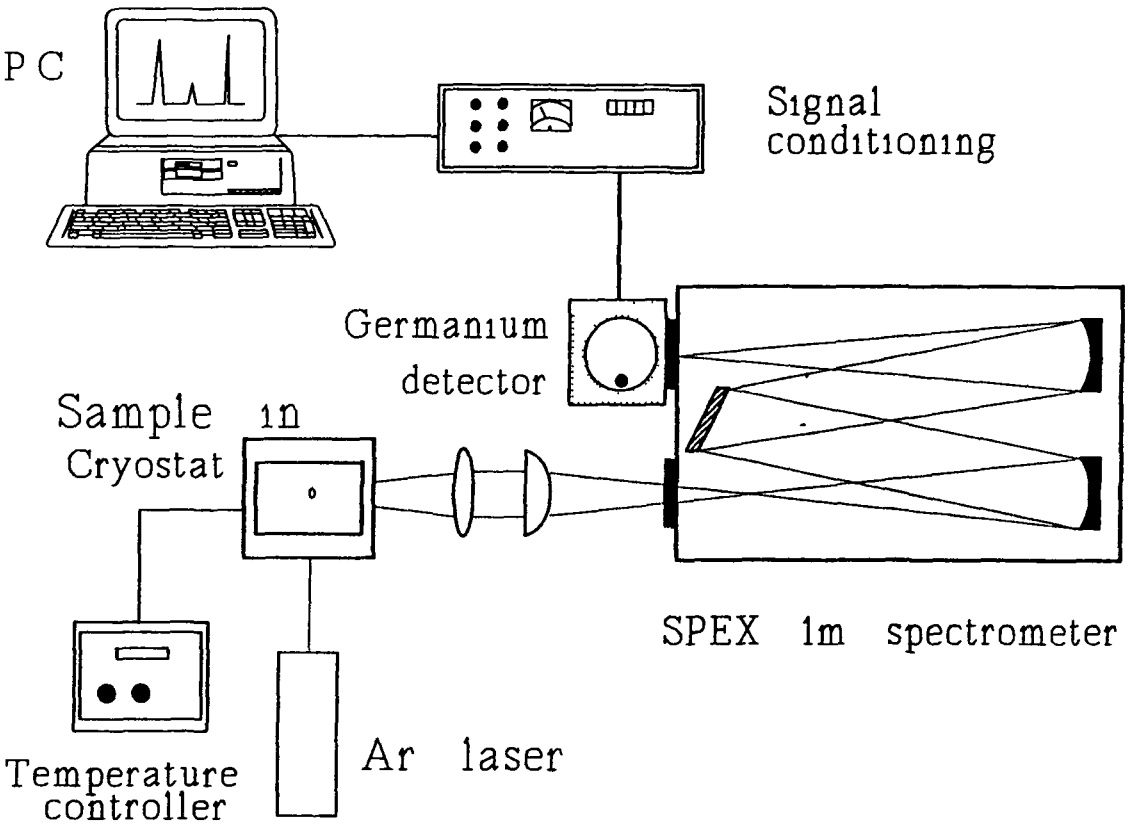

Figure 3 1 Photoluminescence experimental system.

3.4 The stress rig

Uniaxial stress experiments involve compressing an orientated sample along one of the major crystallographic directions For good results care must be taken in the preparation and alignment of the sample and in the design of the apparatus used for applying the stress The ends of the sample must be flat and parallel to each other and perpendicular to the required crystallographic direction The force must be applied normally to the sample ends and without torque, otherwise inhomogeneous stresses could occur which could unnecessarily broaden the no-phonon line or could crack or break the sample A schematic diagram of the system used to apply uniaxial stresses to the oriented samples, for the work reported here, is shown in Figure 3 2

An oriented sample was mounted between two steel pistons with ground flat surfaces in such a way that the long axis of the sample was perfectly perpendicular to the pistons' surfaces and parallel to the vertical axis of the stress cell Double sided adhesive tape was used to hold the samples in position and to act as gaskets to take up any residual roughness A long push-rod rested on the upper piston and extended out of the stress cell to where a force could be applied to it The push-rod was made from hollow tubing to minimise heat transfer from the room to the sample. The force was produced by turning the threaded bar which compressed a steel spring. A Bofors KRA-1 piezoelectric load cell, mounted between the compressed spring and the push-rod, produced an output voltage proportional to the applied force (0 3 mV per 1 kg load). A steel ball bearing retained in the bottom of the load cell prevented any torque generated by the twisting action of the threaded bar from being transmitted to the sample along the push-rod

The load cell was calibrated using a series of standard weights The output was found to be linear, giving an output voltage of 0.286 mV per 1 kg applied An error in the voltage reading of ± 0 001 mV would give an associated error of approximately 0 4% in the stress measurement This is not a significant source of error The relationship between the measured load cell output voltage and the applied force is given by,

$$F = 9.8 \times (V-V0) / 0\,286$$

where F is the force acting on the load cell and transmitted to the sample, V0 is the offset voltage for zero stress and V is the output voltage from the load cell under the applied load The stress on the sample, in MPa, is given by,

$$\text{Stress (MPa)} = 9\,8 \times (V-V0) / 0\,286 \times A$$

where A is the sample cross sectional area in mm^{-2}.

Uniaxial stress experiments were successfully performed on <100>, <110> and <111> oriented samples. The results of these experiments are presented in Chapter 4

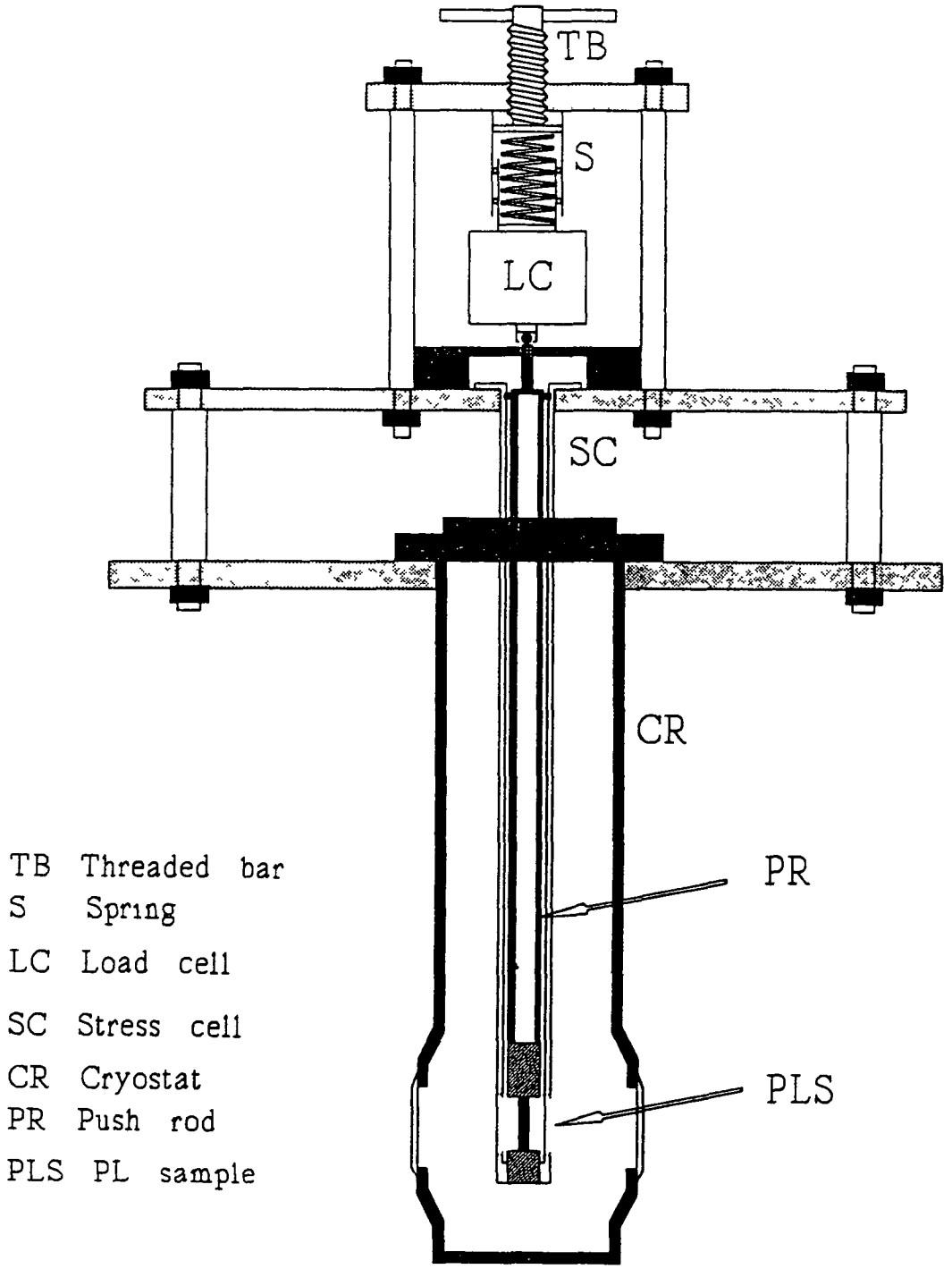

Figure 3.2 The uniaxial stress apparatus

Chapter 4 Results

4.0 Introduction

Alves et al [36,37] in their studies of the epitaxial regrowth, diffusion and lattice location of indium implanted in silicon and in arsenic-preamorphised silicon found that the regrowth and lattice location were very dependent on the crystal type, annealing treatment and crystal orientation They showed that after the implantation of indium in crystalline (100) silicon the highest fraction of indium atoms incorporated into regular lattice sites was about 50%, which was achieved after annealing at 550°C In the case of indium implanted in As-preamorphised silicon 95% of the implanted indium was incorporated into substitutional sites, also achieved after annealing at 550°C. Alves et al. [37] argued that the increase in the fraction of implanted indium in regular lattice sites was related to the formation of In-As pairs These results led to the first attempt to correlate the PAC and PL techniques. The aim was to look for a PL signal which could be identified with In-As pairs in order to confirm the role of In-As pair formation in the increased substitutionality of implanted indium in As-preamorphised silicon Samples of indium implanted silicon and As-preamorphised silicon were annealed at 550°C and low temperature PL spectra were taken The PL spectra of the indium implanted preamorphised silicon showed only already known radiation damage related luminescence lines. No new PL lines which might have been associated with In-As pairs were observed. Thus these defects were deemed unsuitable as a subject for a study of the correlation of the PAC and PL techniques. However, a new PL system,

not previously reported in the literature, was observed in the PL spectra of the indium implanted crystalline silicon samples. This new system was thought to be due to some indium-implantation damage related defect. The PL characterisation of this defect and the identification of the defect as one of a number of defects previously observed using the PAC technique is the subject of the work presented here.

4.1 A new In-implantation damage related PL system

A low temperature photoluminescence spectrum of indium implanted silicon, annealed for two hours, is shown in Figure 4.1. The features labelled P,C and H are luminescence lines arising from known irradiation damage associated defects. These lines are well documented in the literature [2] and are identified in Table 4.1.

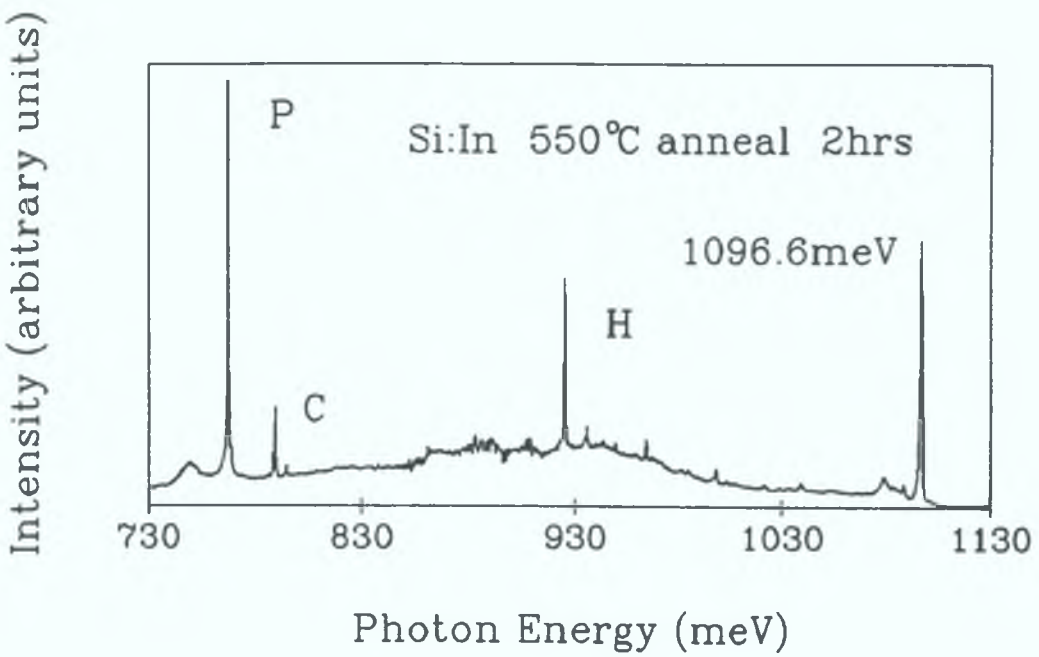

Figure 4.1 A low temperature photoluminescence spectrum of In implanted Si. The features labelled are discussed in the text.

Label	Energy (meV)	Identification
P	767 3	Monoclinic I C-related centre produced by radiation damage and annealing
C	789 4	Monoclinic I radiation damage centre involving C and O
H	925 5	Monoclinic I centre with dependence on C produced by radiation damage and annealing

Table 4 1 Identification of the damage lines labelled in Figure 4 1

The feature labelled 1096 6 meV in Figure 4.1 is a new luminescence system observed in indium implanted silicon. It consists of a strong sharp no-phonon (NP) line at an energy of 1096 6 ± 0 1 meV with an associated structured sideband A detailed spectrum of the 1096 6 meV system is shown in Figure 4.2 The phonon sideband to the low energy side of the NP line arises from electronic transitions assisted by the emission of phonons of various energies. Peaks in the phonon sideband can be identified with peaks in the phonon density of states for silicon The energy regions associated with transverse acoustic (TA) and transverse optic (TO) phonon assisted replicas and the O^{Γ} cutoff are labelled accordingly in Figure 4 2. The preferential coupling observed for the low energy acoustic phonon modes is consistent with a heavy atom like indium being involved in the centre The measured energy separation of the main phonon peaks from the NP line are compared with accepted values of phonon energies in Table 4.2 The two small peaks, seen in Figure 4 2, below the O^{Γ} cutoff energy may be due to two-phonon assisted transitions where, for instance, a TA

momentum-conserving phonon may be emitted together with a k=0 O^{Γ} phonon It is difficult, from the spectra recorded, to precisely identify these features An estimate of the Huang-Rhys factor S, which gives an indication of the electron-phonon interaction at the defect, was made by measuring the intensity of the no-phonon peak (I_0), the total intensity of the phonon side band (I_p) and using the expression [2],

$$I_0 / (I_0 + I_p) = e^{-S}$$

Values of I_0 ~ 2 15 and I_p ~ 1 25 (in arbitrary units) were found for the relevant intensities, which yield

$$I_0 / (I_0 + I_p) = 0\,63$$

$$\Rightarrow \quad S \approx 0\,5$$

The significance of this value of S will become apparent when the origin of the exciton binding energy is discussed in Section 4 2

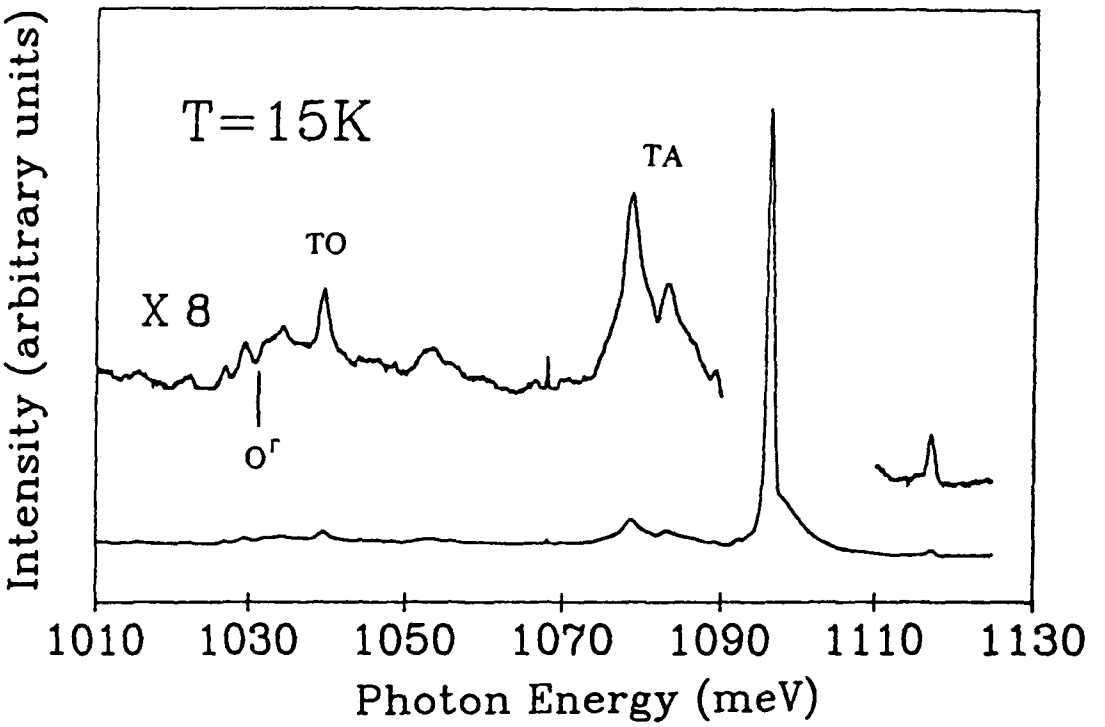

Figure 4 2 A detailed photoluminescence spectrum of the 1096 6 meV system

Separation from NP line (meV)	Possible phonon identification Label	Energy (meV)*
13.3	TA (L3)	14 1
17 8	TA (X3)	18 6
56.8	TO (X4)	57.5
64.1	O^{Γ} cutoff	64 2

Table 4 2 Possible identification of phonon peaks seen in the 1096.6 meV system. * these values are given in reference [46].

The 1096 6 meV no-phonon line is very close in energy to the free exciton TO,LO phonon assisted peaks at 1096 54 meV and 1098 28 meV These peaks (unresolved) are seen as a small shoulder on the high energy side of the NP line in Figure 4 2 The relative intensities of the 1096.6 meV line and the free exciton lines were found to be dependent on the sample temperature and the light source used to excite the PL. For example, spectra taken at 11 K and 20 K, using the white light from a xenon arc lamp filtered through a monochromator as an excitation source, are shown in Figure 4 3(a) and (b), while two spectra taken at the same temperatures but using the 514 5 nm line of an argon ion laser as the excitation source are shown in Figure 4.3(c) and (d) The difference in the spectra can be explained by assuming that the centre responsible for the 1096 6 meV luminescence is associated with implantation damage, which is produced near the surface of a sample during the implantation process. Thus the concentration of centres responsible for the 1096 6 meV luminescence is greater near the surface When using the Ar laser as the excitation source the luminescence from the defect is increased and from the free excitons is decreased, because the wavelength of the light is such that most of it is absorbed in the surface layers of the sample where the concentration of implantation damage is higher; so free excitons are more likely to be trapped at a defect than to recombine giving rise to free exciton luminescence With the Xe lamp as excitation source the light penetrates further into the bulk of the sample, away from the implantation defects where free excitons are more likely to radiatively recombine than be trapped at defects, so the luminescence from free exciton recombination dominates To maximise the defect luminescence the Ar laser was used as the excitation source for the work reported in the following sections. The effects of sample temperature are discussed in Section 4 2

It should be noted that a luminescence line at an energy of 1096 2 ± 0 3 meV has been reported by Obodnikov et al [38] in photoluminescence studies of hydrogen-containing complexes in proton and H_2^+ irradiated silicon This however is purely accidental as the hydrogen related defect anneals out at 400°C while the 1096 6 meV system is still present at annealing temperatures up to 700°C

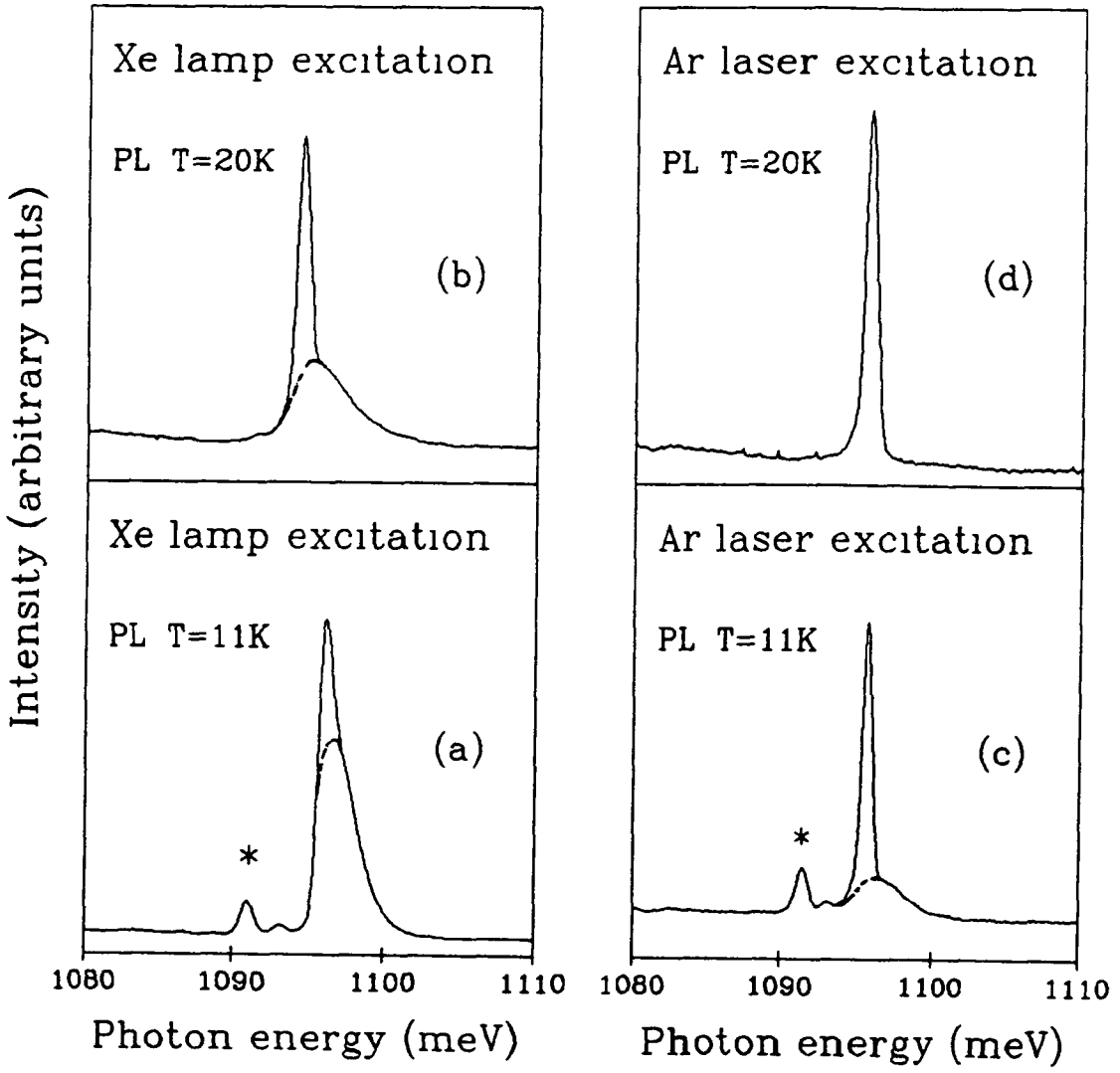

Figure 4 3 Some PL spectra taken at the temperatures indicated, using Xe lamp as excitation source (a), (b) and Ar laser (c), (d) The features labelled * are boron related The dotted lines indicate the position of the FE lines.

4.2 Temperature dependence of the 1096.6 meV system

The temperature dependence of the 1096 6 meV system was investigated by first cooling a sample down to liquid helium temperatures ~ 4 2 K and then heating the sample up by degrees taking PL spectra at regular intervals, until the intensity of the NP line decreased to a level where it was no longer detectable

Some representative PL spectra taken at different temperatures are shown in Figure 4 4 The peak intensity of the 1096 6 meV no-phonon line is plotted as a function of temperature in Figure 4 5

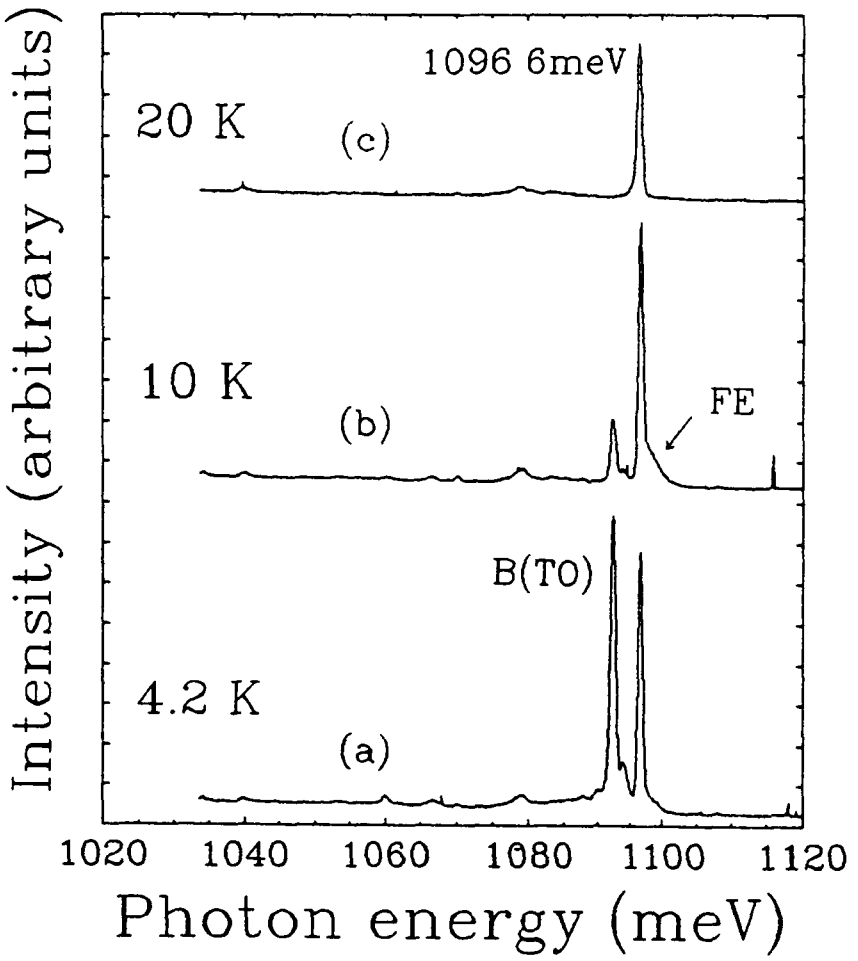

Figure 4.4 PL spectra of the 1096.6 meV system taken at 4 2 K, 10 K and 20 K.

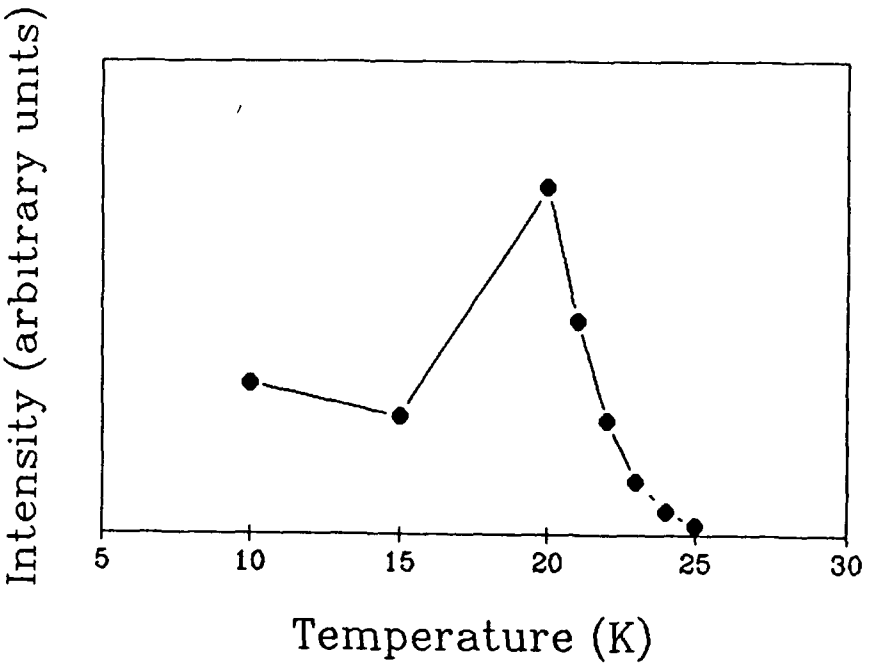

Figure 4 5 Intensity of the 1096 6 meV NP line as a function of temperature

The observed behaviour of the intensity of the 1096.6 meV system is typical of the luminescence arising from the radiative recombination of excitons bound to deep optical centres as discussed in Chapter 1, Section 1 3 2

Figure 4 4(a) shows a PL spectrum taken at 4 2 K The 1096 6 meV NP line and phonon sideband are seen, together with a boron bound exciton TO phonon assisted line (B(TO)). At this low temperature there is no luminescence contribution from free exciton recombination as the majority of the electron-hole pairs created are captured by deep centres like the 1096.6 meV system or shallow centres like the boron acceptor where they recombine radiatively or through non-radiative processes. This accounts for the relatively strong boron related luminescence seen in Figure 4 4(a) As the

temperature is increased the excitons which are loosely bound to the shallow centres begin to thermally dissociate, more electron-hole pairs are then available to be captured at the deeper centres This is reflected in the PL spectrum taken at 10 K where the intensity of the B(TO) peak is reduced with respect to the 1096.6 meV NP line, see Figure 4 4(b) At this temperature there is also a small luminescence contribution from free exciton recombination As the temperature is increased further only the luminescence arising from the recombination of the excitons which are more tightly bound to the deep centres remains. A PL spectrum taken at 20 K, Figure 4.4(c), shows only luminescence from the 1096 6 meV system Above 20 K the intensity of the 1096.6 meV system rapidly decreases to zero

In the bound exciton scenario, two simple reasons can be put forward to explain the rapid decrease m intensity above 20 K either a thermal equilibrium exists between the excitons captured by the deep centre and the free excitons or the excitons thermally dissociate before they can be captured In either case, if E is the relevant ionisation energy, the probability of luminescence is given by [2]

$$I(T)=I(0) / (1+Gexp(-E/kT)) , \qquad (4.1)$$

where G is the effective density of band continuum states into which the ionisation occurs, assuming G and the probability of capturing an exciton at the centre are independent of temperature over the temperature range of interest. It can be shown that, since Gexp(-E/kT) is typically >> 1, equation 4 1 can be rearranged to give

$$Ln\{I(T)/I(0)\} = -ln\ G + E/kT \qquad (4.2).$$

An approximate value for the ionisation energy, E, can be deduced from experimental data by fitting equation 4 2 to the straight line portion of a graph of Ln{I(T)/I(0)} versus 1/T Figure 4 6 shows a graph of Ln{I(T)/I(0)} versus 1/T for the experimental data shown in Figure 4.5. The straight line is a best fit to the high temperature regime data, from which an ionisation energy of 33 8 ± 0 9 meV was calculated This value of E=33 8 meV is larger than the binding energies of excitons bound to ordinary donors or acceptors (eg B (3.8 meV), P (4 7 meV)) but it is similar to values found for the binding energies of the more loosely bound particle of excitons bound to isoelectronic centres [44,2] The total binding energy of the exciton with respect to the free exciton energy (~ 1155 meV) is ~ 58 meV The electron binding energy has been seen to be ~ 34 meV. To account for the remaining ~ 24 meV binding, we note that use can be made of the result that the relaxation energy in the exciton is given by $S\hbar\omega$, where $\hbar\omega$ is the dominant phonon energy and S is the Huang-Rhys factor [2] The sideband has been shown to consist of a large spread of phonon energies with an estimated weighted average of 32 meV Using S ~ 0 5 gives a relaxation energy of 16 meV In view of the approximations made this could account for the remaining binding of the exciton Although there are no lifetime measurements or Zeeman data to help fully identify the centre, it is suggested that the 1096 6 meV system arises from the radiative recombination of excitons bound to electrically neutral traps.

Considering the observed temperature dependence of the 1096 6 meV system a nominal sample temperature of 15 K was used to provide an optimum PL signal in the subsequent annealing and uniaxial stress experiments.

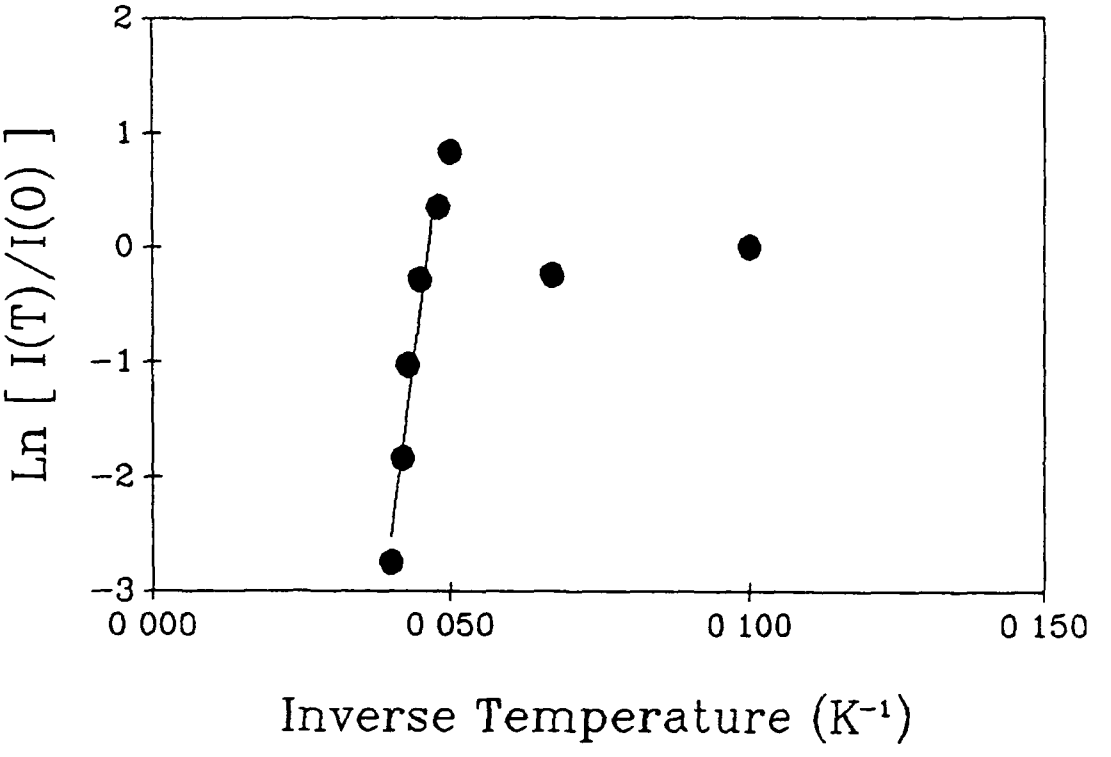

Figure 4.6 Graph of Ln{I(T)/I(0)} versus 1/T for the data shown in Figure 4 5.

4.3 Annealing behaviour

To get some indication of the annealing properties of the 1096 6 meV system, samples of indium implanted silicon were annealed for 15 minutes in the temperature range 200°C to 750°C In the PL spectra of these samples, in addition to the 1096 6 meV system, which first appeared after annealing at 400°C and was annealed out after 650°C, several luminescence lines were observed which are known to arise from defects produced by irradiation damage and heat treatments. These are labelled according to accepted notation (see Davies [2]) in Figure 4 7 which shows some typical spectra recorded after annealing at the temperatures indicated

A graph of the annealing behaviour of the 1096.6 meV system is shown in Figure 4 8, where the normalised intensity of the 1096 6 meV no-phonon line is plotted as a function of the annealing temperature The system was first observed after annealing at 400°C. The luminescence intensity dropped after annealing at 450°C and was seen again between 550°C and 650°C The reason for the drop in intensity at 450°C is unknown It may have been that the defect responsible for the luminescence was temporarily altered in some way between 450°C and 550°C. For instance, a lattice defect, such as interstitial carbon or oxygen, may have become mobile at 450°C and attached itself to the original defect, forming a new defect. At a higher annealing temperature this extra defect may have dissociated from the new defect leaving the original defect behind, this would produce the observed drop in the PL intensity. However, the drop may also have been due to the competitive nature of PL For above-bandgap excitation, as opposed to excitation directly into the defect levels, PL is a competitive process, with a number of different decay channels available for the

recombination of electron-hole pairs (see Figure 1 5, Chapter 1, Section 1.3.1). It may have been that other optical centres or centres involving non-radiative processes were produced between 450°C and 550°C which were more efficient at capturing excitons, this would also result in a decrease in luminescence intensity No further evidence was obtained for either of the above arguments during these annealing experiments More detailed annealing studies would have to be performed to positively identify the phenomenon Despite this and the fact that the particular PL experimental conditions used for this study did not allow the absolute concentration of defects, for a particular annealing temperature, to be determined, the data presented does give a good indication of the temperature range of interest for the annealing of the defect responsible for the 1096.6 meV system

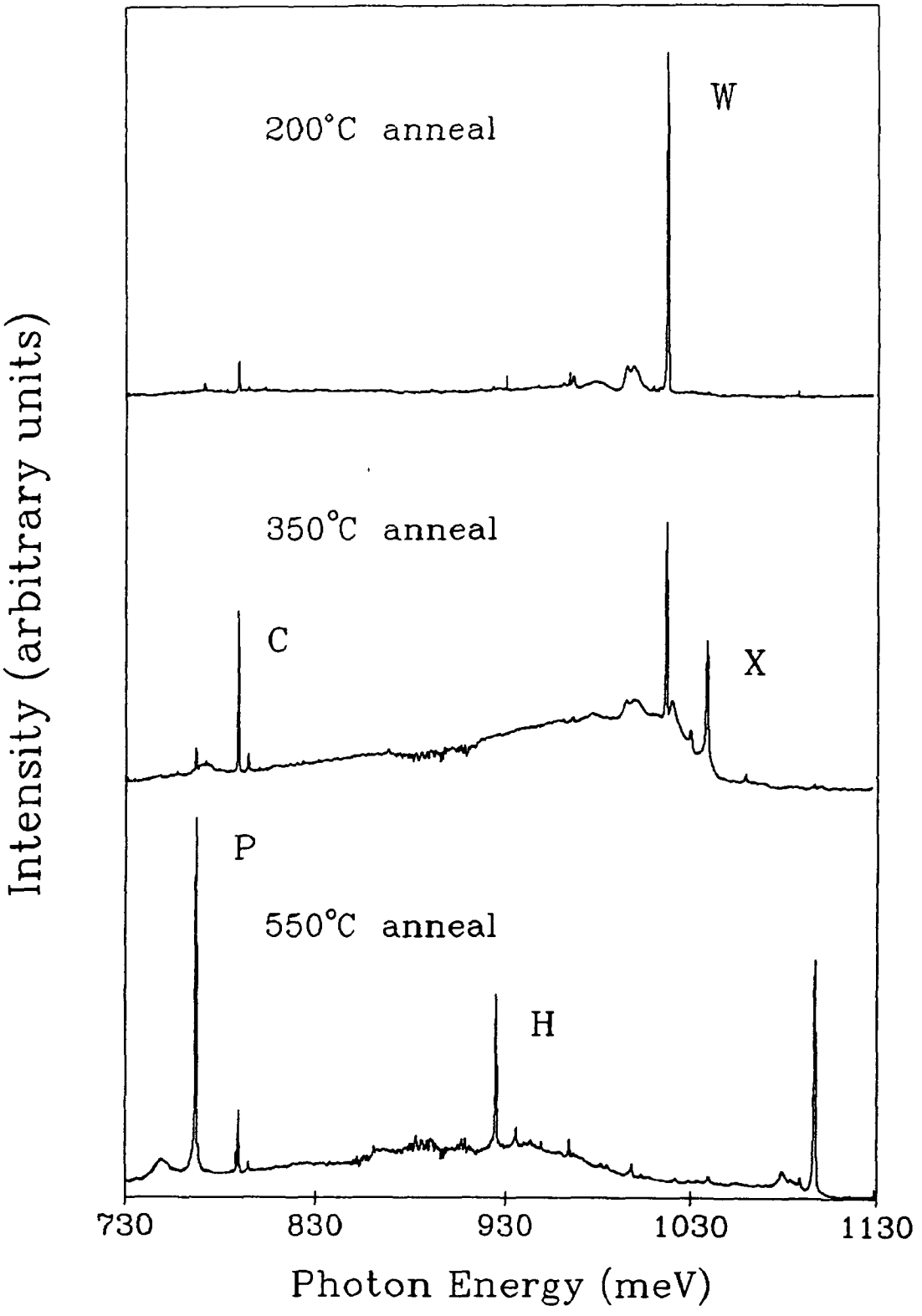

Figure 4.7 PL spectra recorded after annealing In implanted Si at the temperatures indicated. The labelled features are identified in [2].

After annealing at the higher temperatures it was found that as the intensity of the 1096 6 meV system decreased the intensity of the PQR system, the well known In-related isoelectronic centre [19], increased The increase in the intensity of the PQR system is probably observed as indium atoms freed from the 1096 6 meV centre become available to form the PQR centre This gives further evidence of the role of indium in the centre responsible for the 1096 6 meV system.

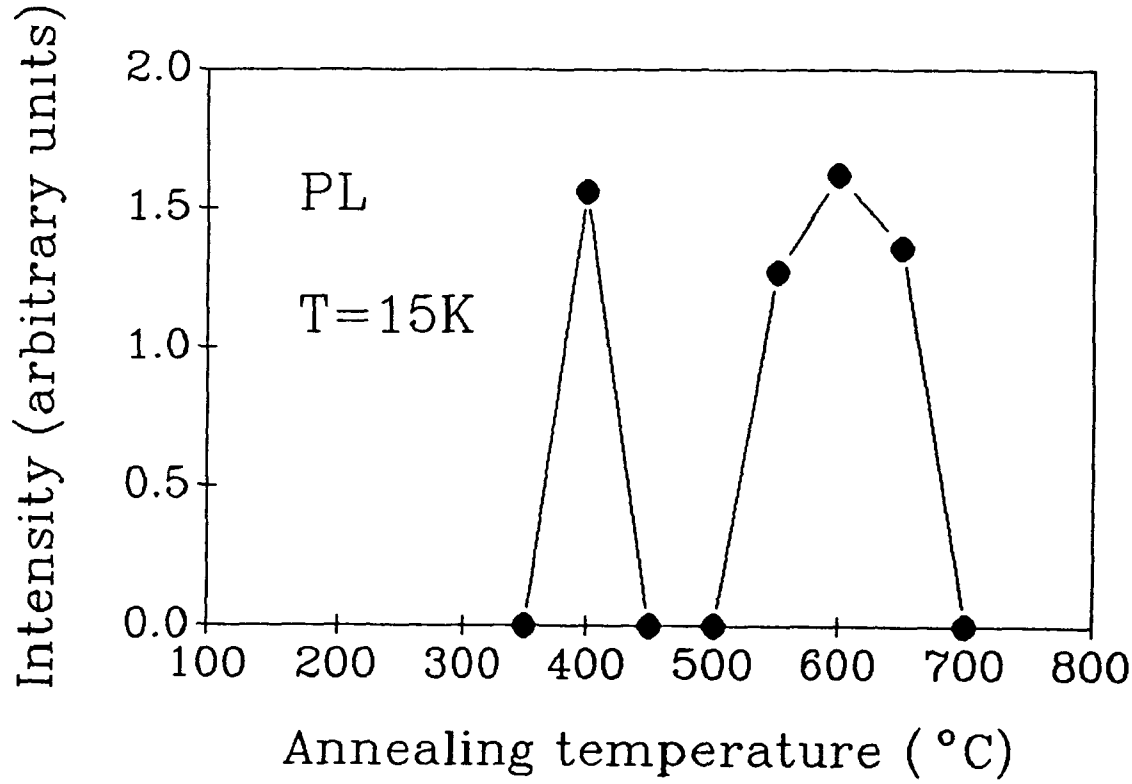

Figure 4.8 Summary of the annealing behaviour of the 1096.6 meV system.

4.4 Uniaxial stress results

Uniaxial stress experiments were performed on a set of oriented silicon samples using the experimental apparatus and procedure described in Chapter 3, Section 3 4 These experiments were designed to provide information on the symmetry of the electronic states involved in the transitions which produce the 1096 6 meV luminescence system and by inference on the symmetry of the atomic structure of the optical centre where the luminescence occurs The results of these experiments are detailed in the following sections

4.4.1 Stress parallel to <111>

When stress was applied in the <111> direction the 1096 6 meV NP line split into two components. Some representative PL spectra showing the splitting of the NP line with different values of applied stress are shown in Figure 4 9 A fan diagram showing a graph of the shift in energy of the two stress-split components as a function of applied stress is shown in Figure 4 10 It can be seen in Figure 4 10 that the shift rates of the stress split components for stress applied in the <111> direction are linear.

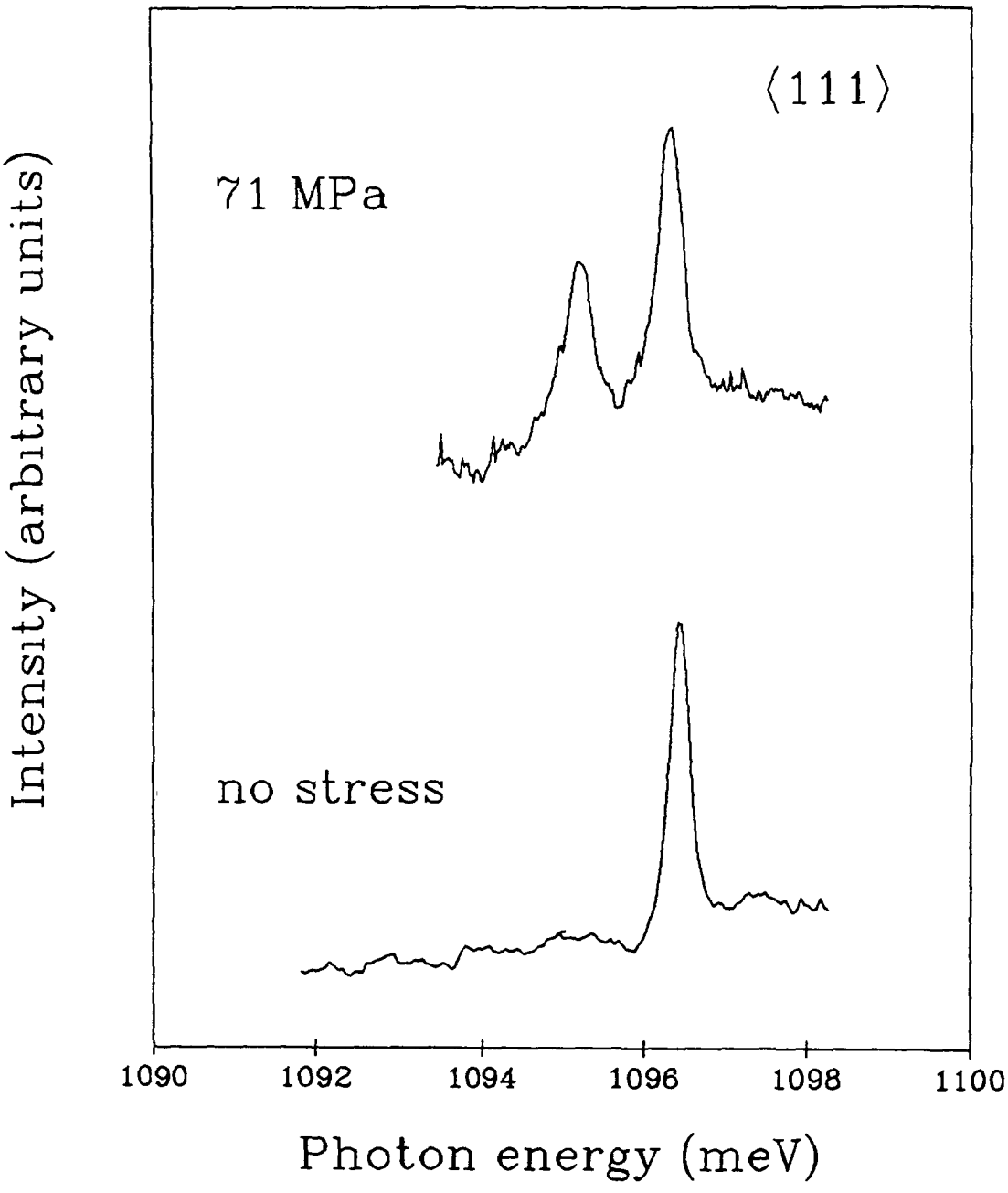

Figure 4.9 PL spectra taken at different values of stress in the <111> direction.

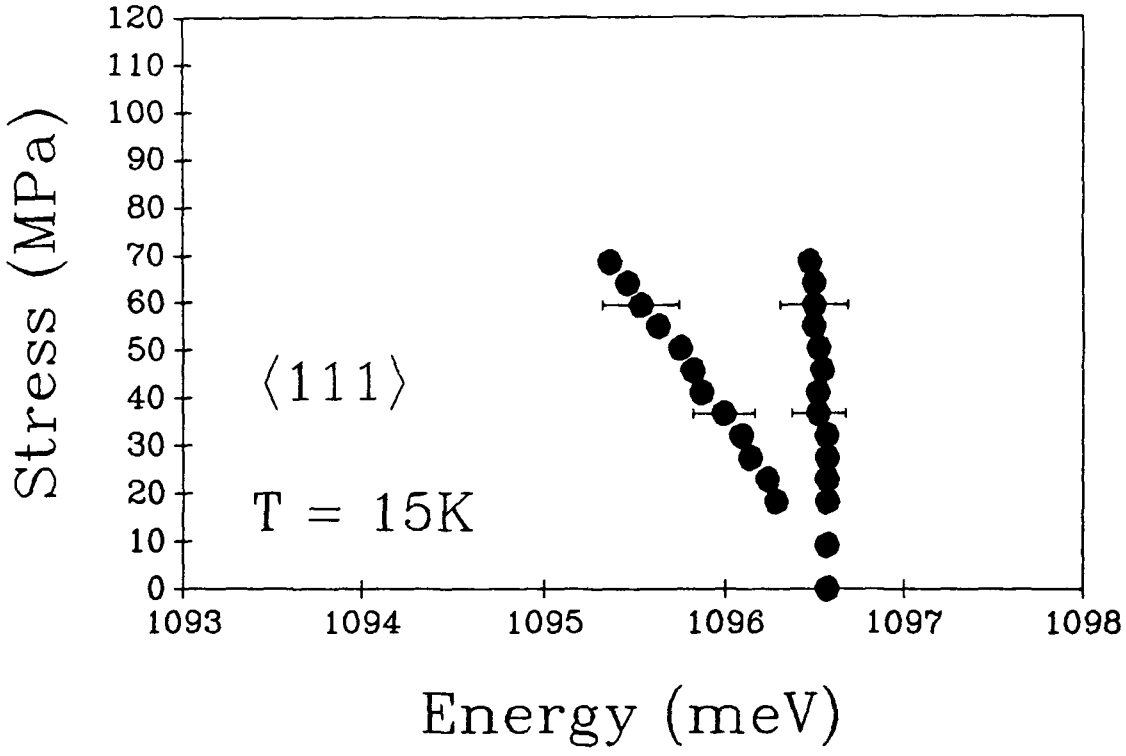

Figure 4 10 Summary of stress induced shifts for stress in the <111> direction The error bars indicate the width of the spectral lines.

4.4.2 Stress parallel to <110>

The 1096 6 meV no-phonon line also split into two components for stress applied in the <110> direction. PL spectra recorded for two values of applied stress are shown in Figure 4 11. The data in Figure 4.12 show that the two components shift to lower energies with increasing applied stress. In contrast to the data for the <111> direction the shift rates for the stress split components for the <110> direction appear to be slightly non-linear It will be seen that the energy shift for stress applied in the <100> direction is highly non-linear. This non-linearity in the shift rates is indicative of interacting energy levels and will be discussed later.

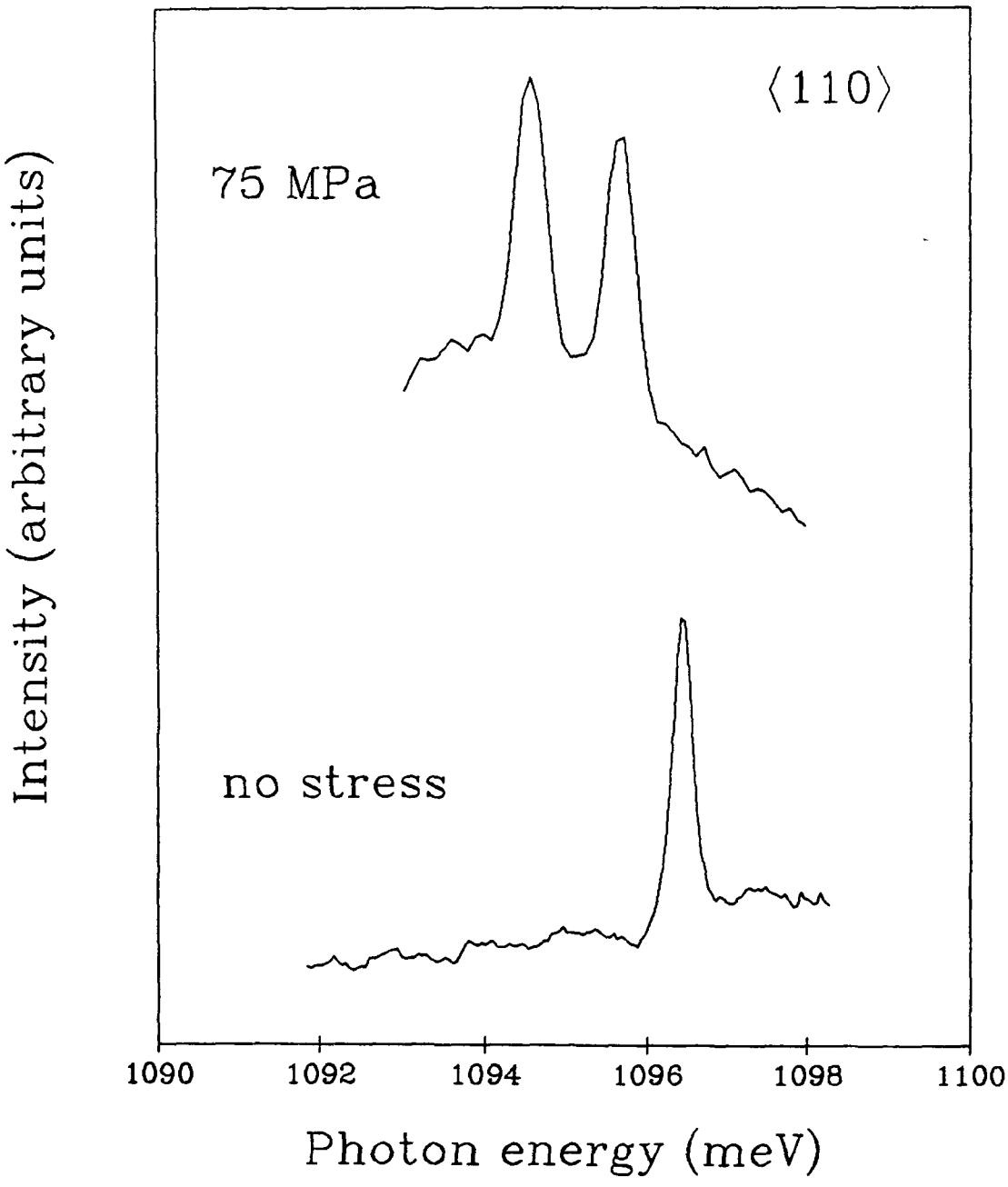

Figure 4 11 PL spectra taken at different values of stress in the <110> direction.

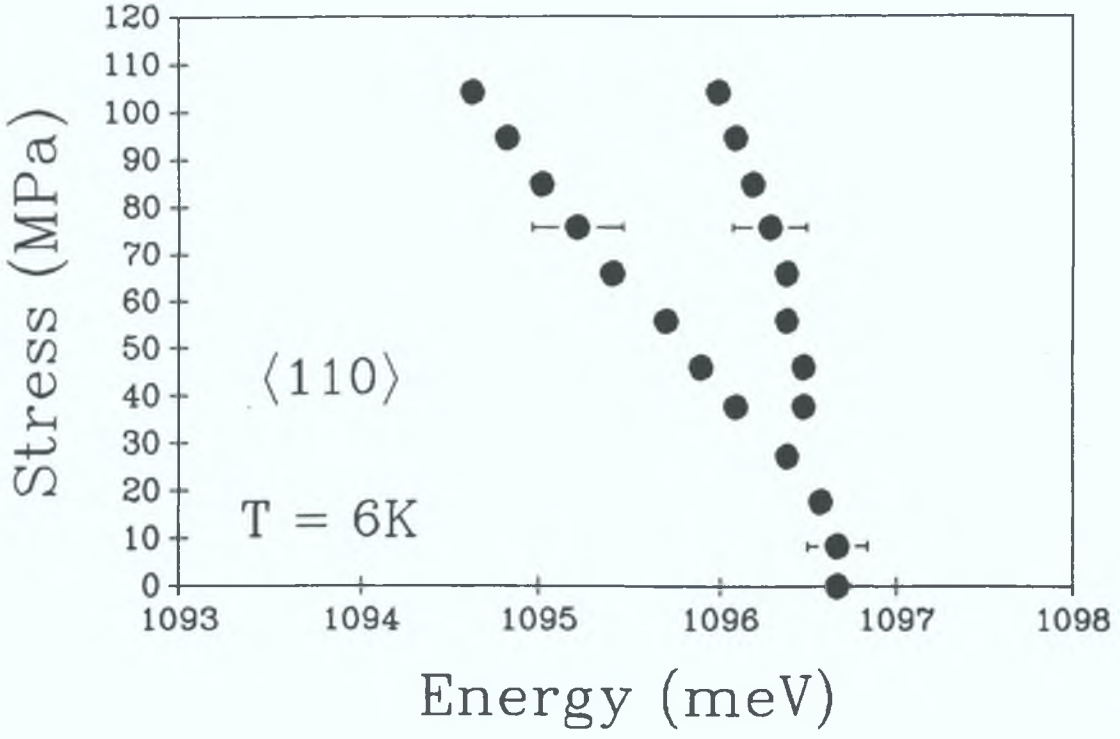

Figure 4.12 Summary of stress induced shifts for stress in the <110> direction. The error bars indicate the width of the spectral lines.

4.4.3 Stress parallel to <100>

Stress applied in the <100> direction did not split the NP line. The line did, however, rapidly shift to lower energies with increasing applied stress. Figure 4.13 shows some spectra taken for particular values of applied stress while the data in Figure 4.14 show the behaviour of the line over a range of stress values. The non-linearity of the shift rate for stress applied in the <100> direction can be clearly seen in Figure 4.14.

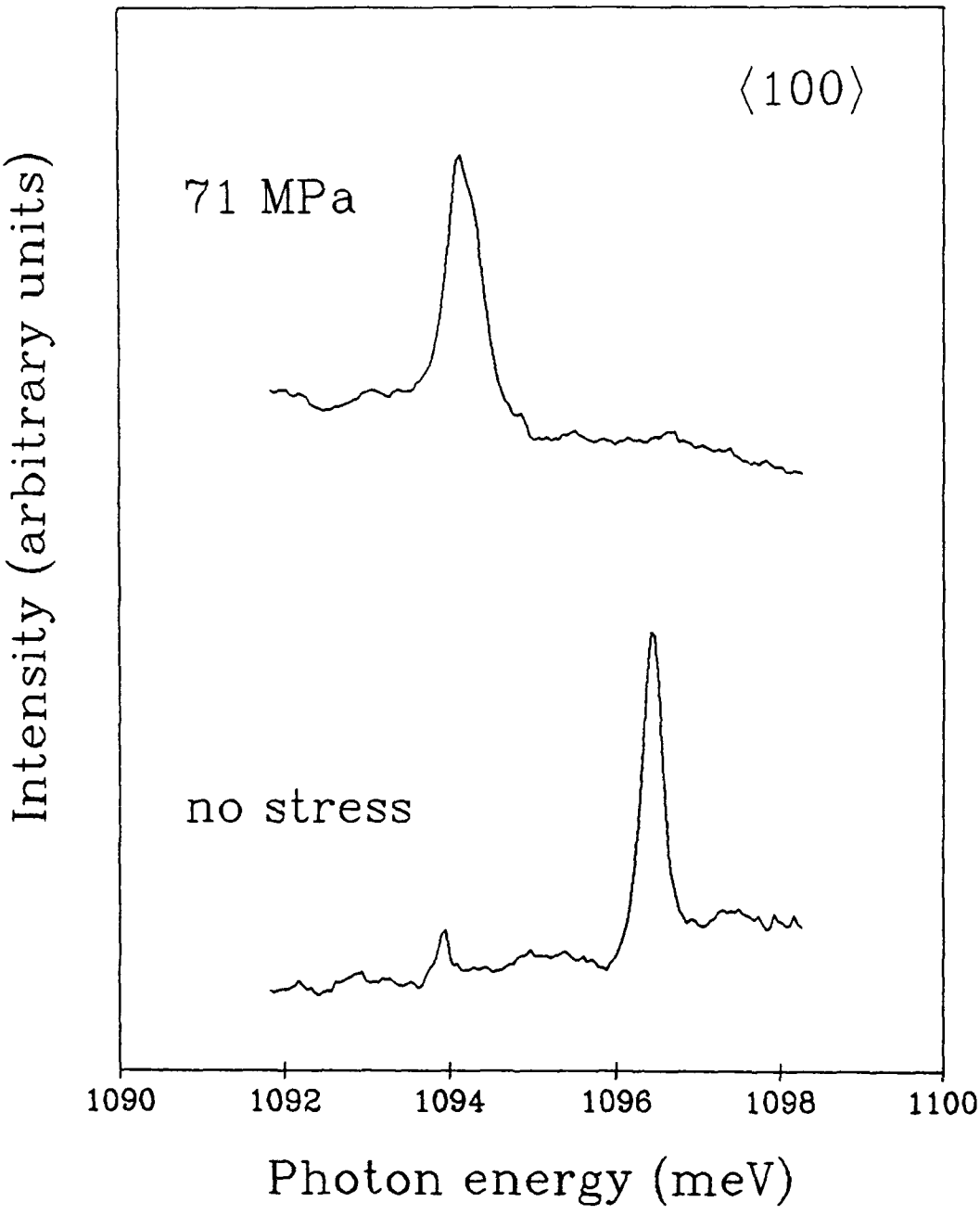

Figure 4 13 PL spectra taken at different values of stress in the <100> direction.

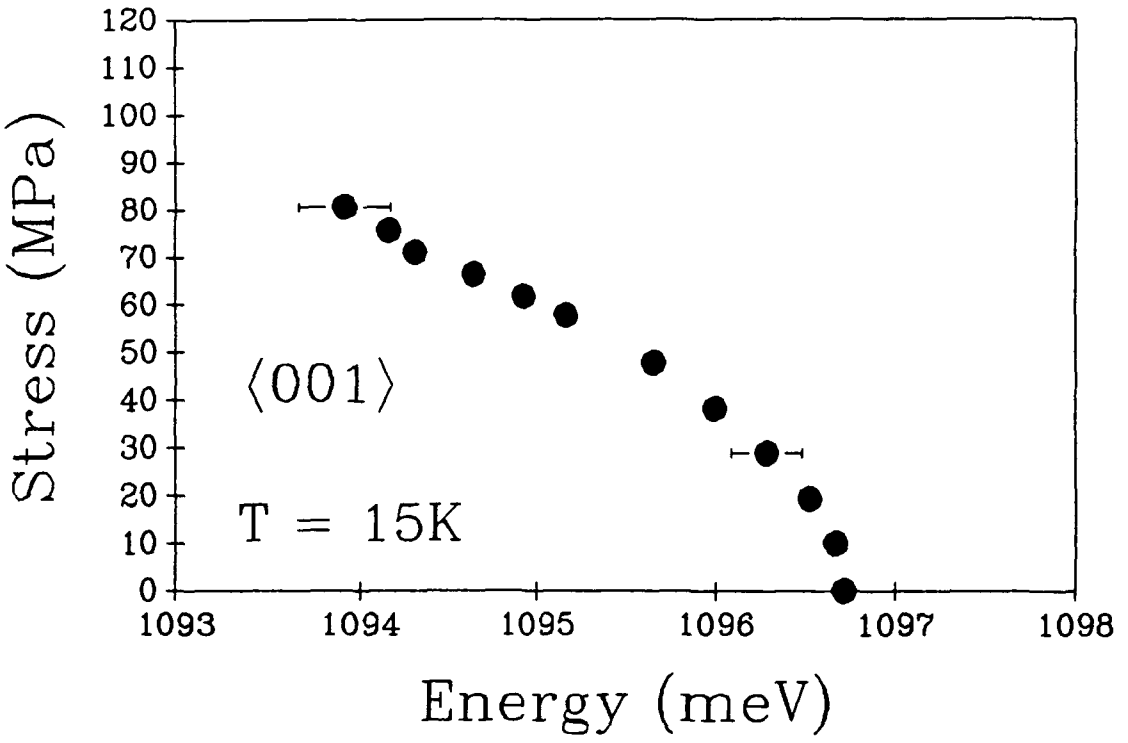

Figure 4.14 Summary of stress induced shifts for stress in the <100> direction The error bars indicate the width of the spectral lines

4.4.4 Polarisation data

Information on the polarisation, with respect to the stress direction, of stress split components can be very useful in identifying the individual components with theoretically derived shift rate parameters It is not always possible, however, to determine the polarisation of a luminescence signal. the polarisation can be mixed by internal reflections in a sample and by stress induced interactions or mixing of states

As a consequence the polarisation data obtained for the experiments reported here are not completely unambiguous It was found that for the two stress split components seen for stress applied in the <111> direction the high energy component was polarised mainly perpendicular to the stress direction while the low energy component was of mixed polarisation The two components seen for stress in the <110> direction and the component for stress in the <100> direction were of mixed polarisation. Figure 4.15 shows some spectra recorded for PL polarised perpendicularly (σ) and parallel (π) to the <111> and <110> stress directions

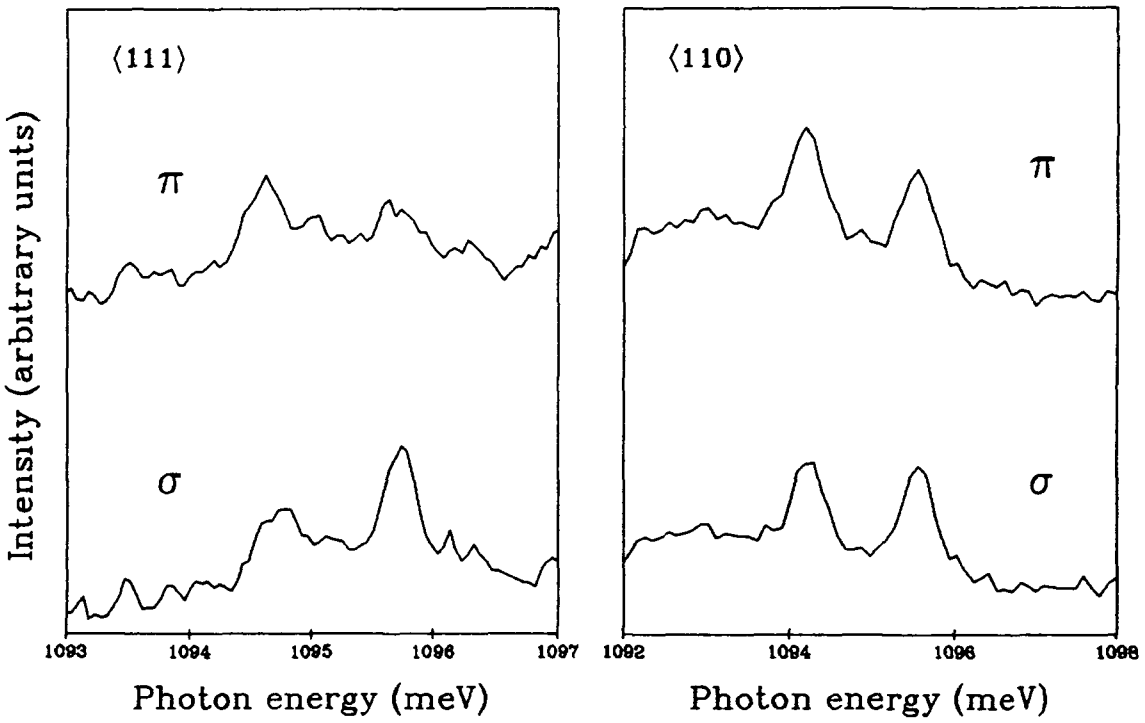

Figure 4 15 Spectra recorded with PL polarised perpendicularly (σ) and parallel (π) to the <111> and <110> stress directions as indicated.

4.5 Analysis of stress results

A summary of the number of stress split components observed for each direction is given in Table 4 3

	Stress direction <111>	<110>	<100>
Number of components	2	2	1

Table 4.3 The number of stress split components observed for each stress direction.

In Chapter 1, Section 1 3 4, a schematic representation of the splittings of no-phonon lines under uniaxial stress for various transitions at centres belonging to the eight possible symmetry systems of a cubic crystal was given in Figure 1 10 Comparing the results in Table 4 3 with the splittings in Figure 1.10 it can be seen that the observed splittings are consistent with the splittings expected for an A to A transition at a trigonal centre. This suggests that the 1096 6 meV no-phonon line arises from a transition between two nondegenerate A states at a trigonal centre and that the splittings under uniaxial stress arise from the removal of the orientational degeneracy of the trigonal centre in the cubic crystal.

Expressions which parameterise the shift rates of optical transitions between nondegenerate states of centres with orientational degeneracy were derived by Kaplyanskii [10,11]. The five shift rates for an A to A transition at a trigonal centre were shown to depend linearly on only two parameters A_1 and A_2 (see Table 1 2, page

20) When the experimentally measured shift rates are linear, values for these parameters can be obtained by fitting the shift rate expressions to the experimental data. For the case of stress applied in the <111> direction the shift rates of the two stress-split components appear to be linear. Using the linear expressions for the shift rates and the slopes of the best fit lines to the data, values of A_1 = -5 95 meV/GPa and A_2 = -6.08 meV/GPa were calculated for the shift rate parameters Using these values and the shift rate expressions for the <100> and <110> directions, the expected linear shifts of the stress-split components for these directions were determined. These are shown as dashed lines in Figure 4 16. The linear fits agree well with the <111> data (they overlap with the solid lines) but do not give good fits for the <100> and <110> directions The noted curvature of the data in Figure 4 16, for stresses applied in the <100> and <110> directions, indicates that the shift rates for these directions are highly non-linear Kaplyanskii's expressions are therefore not appropriate in this case

In an attempt to explain the curvature of the data it should be noted that the six conduction band minima lie along <100> directions and stress applied along one of these directions will produce an overall non-linear effect compression of a silicon crystal along the <100> axis decreases the energy gap in the direction of the compression; but because of a simultaneous dilation in the transverse directions, the conduction band valleys lying in the transverse plane move to a higher energy. Similarly, stress in the <110> direction depresses four of the valleys and raises the other two On the other hand, stress applied in the <111> direction will cause all conduction band minima to shift at the same rate, since the <111> direction makes equal angles with all the <100> directions. If the defect energy levels are closely associated with the conduction band, this type of non-linear behaviour might also be expected for the

defect levels It seems likely, therefore, that the curvature observed for the 1096 6 meV line under <100> and <110> stresses originates in the nature of the conduction band states This is also consistent with the evidence from the temperature dependence of the PL intensity, that the luminescence is due to the recombination of loosely bound electron-hole pairs. The wavefunctions of such loosely bound particles will be predominately band-like, with an envelope function which localises the particles at the defect.

Non-linear shifts of stress split components have been reported for a number of other PL systems [22,39,40]. Such non-linear behaviour is commonly attributed to stress-induced interactions among excited states [22,39,40,41] In photoluminescence excitation (PLE) studies of the excited states of the In-related PQR system under uniaxial stress, Watkins and Thewalt [23] observed linear stress dependence of the stress-split components for stress applied in the <111> direction and notably non-linear dependence for the <110> and especially the <100> directions They argued that such behaviour was suggestive of the valley-orbit effects observed for many shallow donors in Si, in which the electron ground state transforms as A_1 in T_d Unlike the other valley-orbit states E and T_2, A_1 does not split for any direction of stress, but for stresses other than <111>, under which all conduction band valleys are equivalent, the A_1 energy decreases in an initially non-linear manner as the A_1 wavefunction becomes increasingly associated with only the lowest valleys This non-linear shift of the conduction band was previously discussed by Wilson and Feher [42] in electron spin resonance studies of the excited states of donors in silicon, under uniaxial stress Watkins and Thewalt used this argument to show that the excited states of the PQR system, seen in PLE, behave like valley-orbit split shallow donor-like states [23]

The presence of additional excited states is clearly the logical explanation for the curvature of the uniaxial stress data reported for the 1096.6 meV system Unfortunately, the absence of any evidence of such excited states in the PL spectra precludes a satisfactory fitting of the data Nevertheless, it is now shown semi-quantitatively how the curvature of the data arises

The stress Hamiltonian for centres of trigonal symmetry may be expressed as [40,12]

$$\begin{aligned} V = \quad & A_1(s_{xx} + s_{yy} + s_{zz}) + 2A_2(s_{yz} + s_{zx} + s_{xy}) \\ & + B(s_{xx} + s_{yy} - 2s_{zz}) + \sqrt{3}\, B(s_{xx} - s_{yy}) \\ & + C(s_{yz} + s_{zx} - 2s_{xy}) + \sqrt{3}\, C(s_{yz} - s_{zx}) \end{aligned}$$

Here the s_{ij} are stress tensors and A_1, A_2, B and C are electronic operators Following the format adopted by Davies et al [40] for another trigonal centre, a matrix is constructed including interactions between the excited A state and an E state at an energy separation of Δ. The choice of E symmetry for the unseen state is based on two factors Firstly, weakly bound electrons in excitons typically have a ground state of A_1 symmetry with low-lying excited E and T states in tetrahedral symmetry. And secondly, the substantial curvature observed for <001> stresses resembles that for a similar trigonal defect for which interactions with an excited E state were found to be essential to account for the experimental data [40]. The full interaction matrix takes the form,

	A	Ex	Ey
A	α	β	γ
Ex	β	$\delta-\eta+\Delta$	ε
Ey	γ	ε	$\delta+\eta+\Delta$

where $\alpha = A_1(s_{xx} + s_{yy} + s_{zz}) + 2A_2(s_{yz} + s_{zx} + s_{xy})$

$\beta = B(s_{xx} + s_{yy} - 2s_{zz}) + C(s_{yz} + s_{zx} - 2s_{xy})$

$\gamma = \sqrt{3}\, B(s_{xx} - s_{yy}) + \sqrt{3}\, C(s_{yz} - s_{zx})$

$\delta = A_1'(s_{xx} + s_{yy} + s_{zz}) + 2A_2'(s_{yz} + s_{zx} + s_{xy})$

$\eta = B'(s_{xx} + s_{yy} - 2s_{zz}) + C'(s_{yz} + s_{zx} - 2s_{xy})$

$\varepsilon = \sqrt{3}\, B'(s_{xx} - s_{yy}) + \sqrt{3}\, C'(s_{yz} - s_{zx})$

In this matrix the symbols A_1', B' and C' are used for the E state operators Matrices for each stress direction are given in Appendix B Circumstantial evidence from experiment is now used to simplify the analysis Firstly, from Appendix B, it is found that only the C parameter can produce curvature under <111> stress, and since there is at most very slight curvature, C is approximated to zero. Also, the values of A_1 and A_2 already determined from a good linear fit to the <111> data are retained in this analysis, i e. A_1 = -5.95 meV/GPa and A_2 = -6 08 meV/GPa. The absence of any stress data from the proposed E state means that there are no indications of appropriate values for A_1', A_2', B', C' or Δ. The A, B and C parameters are assumed to be the same for the two interacting excited states i.e $A_1' = A_1$ etc The parameters Δ and B are now allowed to vary to seek good agreement with experiment An initial estimate of 5 meV was chosen for Δ - for somewhat smaller separations spectral evidence at temperatures

of ~ 20 K might reasonably have been expected The solid lines shown in Figure 4 16 are obtained for Δ = 7 meV and B = 27 meV/GPa Good agreement with experiment is obtained up to stresses of ~ 50 MPa At larger stresses, substantial deviations are observed Although the model proposed is not adequate to fully account for the experimental data, we believe that the origin of the curvature has been correctly identified

Until further studies, using photoluminescence excitation or absorption spectroscopy, can be undertaken to investigate the excited states of the defect under stress, no fully quantitative analysis can be made of the shift rates of the 1096 6 meV NP line

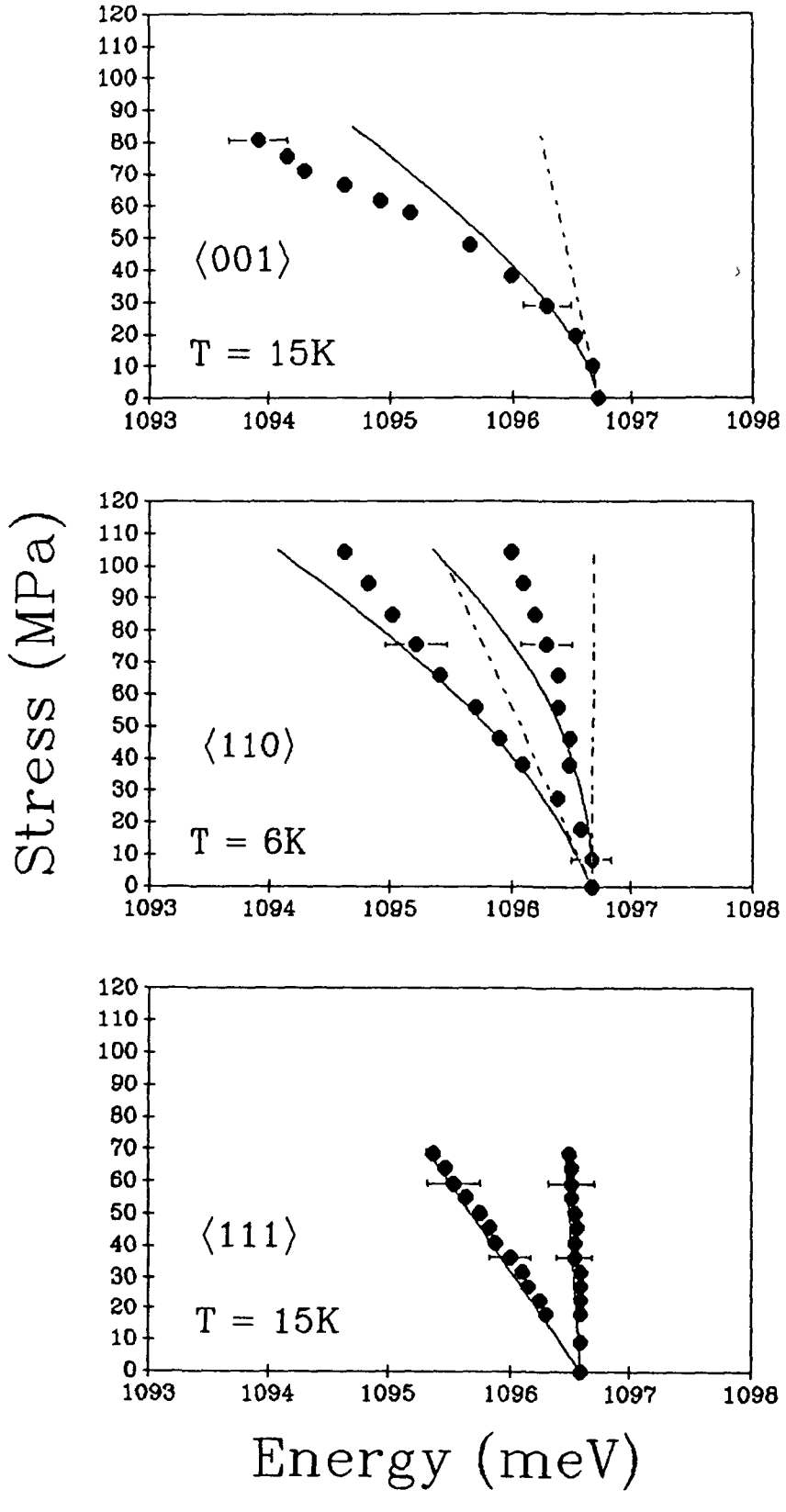

Figure 4 16 Uniaxial stress data with model fits for stress in the <111>, <110> and <001> directions. The dashed lines are the expected linear fits for an A to A transition at a trigonal centre The solid lines are fits obtained taking into account interactions among excited states of the defect.

4.6 Conclusions

When indium implanted silicon is annealed in the temperature range 400°C to 700°C an indium-implantation damage associated defect is produced which gives rise to a new low temperature PL system consisting of a sharp no-phonon line at 1096.6 meV accompanied by a weak phonon sideband. Uniaxial stress experiments show that the defect has trigonal symmetry and that the NP line arises from transitions between two non-degenerate electronic states The evidence suggests that these states are conduction band associated or donor-like states of excitons bound to isoelectronic centres. A semi-quantitative analysis of the uniaxial stress results has shown that the curvature of the data arises through the interactions of excited states of the defect.

Chapter 5 Discussion and conclusions

5.1 Correlation of PL and PAC results

Perturbed angular correlation spectroscopy (PAC) is a nuclear technique which, in recent years, has been applied with some success to the characterisation of defect complexes in semiconductor materials [14] PAC provides information on the atomic structure and annealing properties of defect complexes. The technique, however, suffers from the limitation that it does not directly provide information on the characteristics of the electronic states of the defect, often the technological important factor For PL on the other hand, the electronic states are probed directly by analysing the characteristics of the recombination spectrum and when combined with perturbation techniques such as uniaxial stress and Zeeman measurements PL can provide information on the local atomic configuration of a defect. In favourable cases PL can help to identify not only the element but also the number of atoms of that element which constitute the defect [43].

If it could be shown that the results obtained from certain PAC and PL studies originate from the same defect, the information provided by each technique could be used to give a more complete description of that particular defect. This subject is now discussed in relation to the results of the PL study presented in chapter four

A short review was given in Chapter 2, Section 2.2, of some of the defect complexes which have already been observed in indium implanted silicon using the perturbed angular correlation spectroscopy technique. There were three defects

mentioned in particular, listed in Table 2.2 (page 30) as In-De1, In-De2 and In-De3, which were reported by Wichert et al [14] to be complexes formed by the indium probe atoms with intrinsic lattice defects produced by the implantation process The fractions f_1, f_2 and f_3 of indium atoms in the complexes In-De1, In-De2 and In-De3, respectively, and the fraction f_0, of indium atoms in damage free sites, as observed by PAC during annealing of the implantation damage were plotted in Figure 2 3 (page 31) Considering the annealing behaviour of the three complexes, Wichert et al. [14] proposed that, since the disappearance of one complex coincided with the appearance of the next complex, it might be that the different complexes are formed by the accumulation of defects at a complex of simpler structure In-De3 was thought to have been the smallest of the three complexes, possibly formed by the trapping of a neutral vacancy at the indium probe atom The next complex, In-De1, was explained by the trapping of additional vacancies or impurity related defects, such as C or O atoms, at the In-De3 complex. And the formation of the third complex, In-De2, which was seen to be favoured by high defect densities such as those produced by the implanted probes correlated damage cascade, was thought to occur via the In-De1 complex again by the trapping of additional defects

There is evidence in the results of the PL study of the 1096.6 meV PL centre, presented in chapter four, to suggest that this defect, which was discovered in indium implanted silicon, is also an indium-implantation damage related complex The annealing behaviour of two of the PAC defects, In-De1 and In-De2, are reproduced in Figure 5.1 below, together with the annealing behaviour of the 1096 6 meV centre as seen in PL (discussed in Section 4 3). From a comparison of the annealing properties of the defects shown in Figure 5 1 it appears that there is a direct correspondence

between the 1096 6 meV PL centre and the defect labelled In-De2

These results are not conclusive Wichert et al [14] have given only a preliminary analysis of the PAC data and the PL centre discussed has not yet been fully characterised, however, it seems likely that the results of the PAC and PL studies refer to the same defect complex.

It should be noted that whereas the radioactive indium isotope ^{111}In was used as the probe in the PAC experiments, the PL studies were performed on silicon samples implanted with the stable isotope ^{115}In To help complete the analysis it would be useful to perform PAC and PL on samples with identical indium doses and heat treatments As it is, the results presented so far do indicate that under favourable conditions PL should prove to be a useful technique in providing important complementary information for PAC and other nuclear techniques

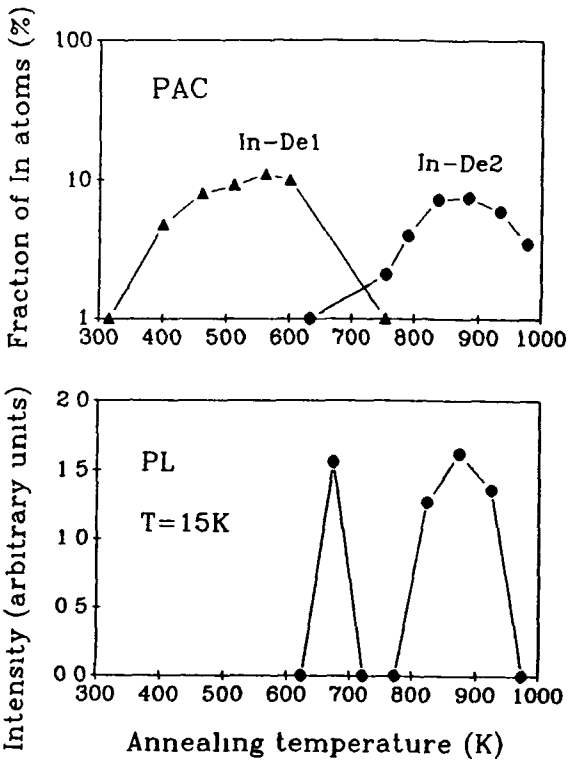

Figure 5.1 The annealing behaviour of the In-De1 and In-De2 defect complexes as seen in PAC (extracted from [14]) and of the 1096.6 meV system as seen in PL.

5.2 A note on the use of radioactive probes

It is envisaged that PL studies on samples containing the same radioactive probes as are used in PAC studies would help to correlate the PAC and PL results This is because it is expected that if a PL spectrum is observed which is thought to originate at a defect complex which involves a radioactive impurity, as the radioactive atoms decay (say from ^{111}In by electron capture to ^{111}Cd) the electronic properties of the defect should change The number of original defects would decrease and a corresponding decrease should be seen in the intensity of the PL spectrum associated with the defect If the product of the decay of the radioactive impurity produces a second defect, a new PL spectrum may appear as the old one disappears This would make it easier to identify a particular PL spectrum with the corresponding defect being studied using PAC.

For the same reasons radioactive substitutes could be used to identify the constituents of a defect Usually in PL studies the presence of a particular element in a defect complex is investigated by intentionally doping a sample with known ratios of different isotopes of the element and then looking for very small energy shifts in the PL spectra, due to the different isotopes This isotope shift technique requires very high resolution spectra, which are not always possible. If a sample was doped with a radioactive isotope of the element the intensity of the PL spectrum should decrease at the rate of the radioactive decay, this change in intensity might be easier to measure than a small energy shift If the element was not involved in the complex no decrease in intensity would be expected. In this way the role of a particular impurity in a defect complex could be investigated.

When using radioactive implants it would be advantageous, for practical considerations, to be able to keep the activity of the sample under investigation as low as possible The question arises as to what concentration of radioactive impurities would be necessary to give a good PL signal and what would be the corresponding activity of the sample ?

PL is a very sensitive technique for which small sample volumes (0 1 mm^3) and low defect concentrations (approx 10^{12} cm^{-3} or less in some cases) are adequate for making measurements Take for example a typical experimental situation· a minimum sample volume of 1 mm x 1 mm x 0.1 mm = 0.1 mm^3 or 10^{-4} cm^3 might be used with a minimum detectable defect concentration of 10^{15} cm^{-3} The number of radioactive impurities required to give this defect concentration would be 10^{15} cm^{-3} x 10^{-4} cm^3 = 10^{11} atoms The activity of a sample containing this number of radioactive atoms is given by,

$$dn/dt = -n\lambda$$

$$\text{where } \lambda = 0.693 / T½$$

Assume, for example, that the half-life is one day,

$$T½ = 8.64 \times 10^4 \text{ sec}$$

$$\Rightarrow \lambda = 8.02 \times 10^{-6} \text{ s}^{-1}$$

$$\therefore dn/dt = -10^{11} \times 8.02 \times 10^{-6} \text{ s}^{-1}$$

$$= -8.02 \times 10^5 \text{ s}^{-1}$$

Recall that 1 mCi $= 3.75 \times 10^{7}$ dps

$\Rightarrow 8.02 \times 10^{5}$ dps $= 2.14 \times 10^{-2}$ mCi

$= 21\ \mu$Ci

This is a modest level of activity and would be well inside the limits of practical working levels. So it is seen that there is a potential for combining the use of radioactive impurities with the PL technique in characterising defect complexes.

5.4 General Conclusions

The results of a PL study of indium implanted silicon have been presented It was shown that annealing in the temperature range 400°C to 700°C produces a defect which gives rise to a previously unreported low temperature PL spectrum. This spectrum consists of a sharp no-phonon line at 1096.6 meV with an associated structured phonon sideband. Peaks in the phonon sideband have been identified with peaks in the density of phonon states for silicon The results of uniaxial stress and temperature dependence measurements indicate that the spectrum arises from the recombination of electron-hole pairs at a centre with trigonal symmetry, and that the optical transition occurs between two nondegenerate electron states. Interactions among excited states of the centre were inferred from nonlinear shift rates observed in the stress measurements, but no optical transitions were detected from these states The

behaviour of the stress induced shift rates suggests that the states are conduction band associated or donor-like in nature

Using the PL results as a case study it was shown that PL should prove to be a useful technique for providing excellent complementary information for PAC and other nuclear techniques, while the use of radioactive impurities could in turn aid in the PL characterisation of defect complexes.

References

[1] S Mader, in Ion Implantation Science and Technology edited by J F Ziegler (Academic Press 1984), p. 109.

[2] G Davies, Phys. Rep 176 (1989) 83

[3] M A Vouk and E.C Lightowlers, J Phys C 10 (1977) 3689

[4] P McL. Colley and E.C. Lightowlers, Semicond Sci. Technol 2(1987) 157

[5] J.J Hopfield, D.G. Thomas and R T Lynch, Phys Rev. Lett. 17 (1966) 312.

[6] E Cohen and M.D Sturge, Phys Rev B 15 (1977) 1039

[7] M A Vouk and E.C. Lightowlers, J Lumin. 15 (1977) 357.

[8] J Weber, W Schmid and R. Sauer, Phys. Rev. B 21 (1979) 2401.

[9] E C Lightowlers in Growth and Characterisation of semiconductors, edited by R.A Stradling and P.C Kilpstein, (Adam Hilger 1990), p 135

[10] A.A Kaplyanskii, Opt. Spectrosc 16 (1964) 329

[11] A A. Kaplyanskii, Opt. Spectrosc 16 (1964) 557.

[12] A E Hughes and W.A. Runciman, Proc. Phys Soc 90 (1967) 827

[13] K. Mohammed, G Davies and A T Collins, J Phys. C 15 (1982) 2779.

[14] Th. Wichert, M. Deicher, G. Grubel, R. Keller, N. Schulz and H. Skudik, Appl. Phys A 48 (1989) 59.

[15] J R. Haynes, Phys. Rev. Lett. 4 (1960) 361.

[16] P.J. Dean, J.R Haynes and W F Flood, Phys Rev. 161 (1967) 711

[17] P.J. Dean, W F. Flood and G. Kaminsky, Phys. Rev. 163 (1967) 721.

[18] G S Mitchard, S.A. Lyon, K.R Elliott and T C McGill, Solid State Commun. 29 (1979) 425

[19] M.L.W Thewalt, U O Ziemelis and R R. Parsons, Solid State Commun 39 (1981) 27

[20] J. Weber, R Sauer and P Wagner, J Lumin. 24/25 (1981) 155

[21] J Wagner and R. Sauer, Phys Rev B 27 (1983) 6568.

[22] S P. Watkins and M L.W Thewalt, Can. J Phys 63 (1985) 1074.

[23] S P Watkins and M L.W Thewalt, Phys Rev B 34 (1986) 2598.

[24] S P Watkins, M L W. Thewalt and T. Steiner. Phys Rev B 29 (1984) 5727.

[25] R.E Stahlbush and R.A Forman, J Lumin 26 (1982) 227

[26] U O Ziemelis, R R Parsons and M Voos, Solid State Comm 32 (1979) 445.

[27] D H Brown and S R Smith, J Lumin. 21 (1980) 329

[28] T G. Brown and P L. Bradfield, Phys Rev. B 37 (1988) 2699.

[29] M L W Thewalt, T. Steiner and J I. Pankove, J Appl Phys 57 (1985) 498.

[30] Th Wichert, E Recknagel in Microscopic Methods in Metals, Topics in current physics, vol 40, edited by U. Gonser (Springer 1986) p 317

[31] E.N Kaufmann, R Kalish, R A Naumann and S Lis, J Appl Phys. 48 (1977) 3332

[32] J C Soares, G Grubel, C Jeynes, B.L. Sealy, M F Da Silva and A A. Melo, Europ. Mat Res Soc. Symp. Proc 15 (1987) 595.

[33] J C. Austin, M L Swanson, W C. Hughes, and S S. Choi, Mat. Res Soc Symp. Proc 209 (1990) 469

[34] R. Keller, M Deicher, W Pfeiffer, H Skudlik, D. Steiner and Th. Wichert, Phys Rev Lett 65 (1990) 2023

[35] Th. Wichert, H Skudlik, H D Garstanjen, T Enders, M Deicher, G. Grubel, R. Keller, L. Song and M. Stutzmann, Mat. Res. Soc. Symp Proc 104 (1987) 265.

[36] E Alves, M F Da Silva, A.A. Melo, J.C. Soares, U. Feuser and R. Vianden, Mater. Sci Eng. B 4 (1989) 189.

[37] E. Alves, M F Da Silva, J.C. Soares, A.A. Melo, J. May, V Haslar, P Seidl, U. Feuser and R. Vianden, Nucl Instrum. Methods B 55 (1991) 580.

[38] V I Obodnikov, L N Safronov and L S Smirnov, Sov Phys Semicond 10 (1976) 815

[39] C P Foy, J Phys C 15 (1982) 2059

[40] G Davies, E C Lightowlers and Z E Ciechanowska, J Phys C 20 (1987) 191

[41] G Davies, Mat Res. Soc Symp Proc 104 (1987) 65

[42] D K. Wilson and G Feher, Phys. Rev. 124 (1961) 1068

[43] L T Canham, G Davies and E C. Lightowlers, J. Phys C 13 (1980) L757

[44] M L W. Thewalt, U O. Ziemelis, S P Watkins, and R.R Parsons, Can J. Phys. 60 (1982) 1691

[45] D B Fitchen, in Physics of Color Centers, edited by W.B Fowler (Academic Press 1968), p 294

[46] K W Boer, in Survey of Semiconductor Physics - electrons and other particles in bulk semiconductors (Van Nostrand Reinhold 1990), p. 100

Acknowledgements

In completing this thesis I would like to thank my research supervisor Dr Martin Henry for all his help which is greatly appreciated Thanks also to the Solid State Group postgrads, postdocs and research assistants past and present who have helped me in one way or another during my research. I would especially like to thank Jim Campion, Siobhan Daly, Dr Kevin McGuigan and Maree.

Appendix A

This appendix contains the cleaning procedure used in the preparation of various samples of silicon for photoluminescence spectroscopy

Silicon sample cleaning procedure

1. Boil in methanol
2. Rinse in cold methanol
3. Boil in trichloroethylene
4. Rinse in cold methanol
5. Rinse in de-ionised water
6. Boil in $NH_4OH.H_2O_2$ H_2O 5:1·1
7. Rinse in de-ionised water
8. Boil in HCl H_2O_2 H_2O 5:1:1
9. Rinse in de-ionised water
10. Blow dry

Appendix B

This appendix contains the general matrix for an A to A transition at a trigonal centre which takes into account interactions between the excited A state and an additional excited E state, as well as the five matrices which describe the behaviour of the stress-split components of the A to A NP line under <111>, <110> and <001> stresses

The general matrix takes the form,

	A	Ex	Ey
A	α	β	γ
Ex	β	δ-η+Δ	ε
Ey	γ	ε	δ+η+Δ

where $\alpha = A_1(s_{xx} + s_{yy} + s_{zz}) + 2A_2(s_{yz} + s_{zx} + s_{xy})$

$\beta = B(s_{xx} + s_{yy} - 2s_{zz}) + C(s_{yz} + s_{zx} - 2s_{xy})$

$\gamma = \sqrt{3}\, B(s_{xx} - s_{yy}) + \sqrt{3}\, C(s_{yz} - s_{zx})$

$\delta = A_1'(s_{xx} + s_{yy} + s_{zz}) + 2A_2'(s_{yz} + s_{zx} + s_{xy})$

$\eta = B'(s_{xx} + s_{yy} - 2s_{zz}) + C'(s_{yz} + s_{zx} - 2s_{xy})$

$\varepsilon = \sqrt{3}\, B'(s_{xx} - s_{yy}) + \sqrt{3}\, C'(s_{yz} - s_{zx})$

The stress tensors s_{ij} are defined as

$$s_{ij} = |s| \, \mathrm{Cos}(\hat{s},\hat{\imath})\mathrm{Cos}(\hat{s},\hat{\jmath})$$

where $|s|$ is the magnitude of the applied stress and $(\hat{s},\hat{\imath})$ is the angle between the direction of the stress and the direction of the crystal axis i For the lifting of the orientational degeneracy, the full family of defects (trigonal in this case) is divided into groups which are in-equivalent with respect to the applied stress Instead of choosing different defects representative of each group to calculate the s_{ij}, we choose a single defect and examine the effects of stress along in-equivalent crystal directions of the same type. Thus, for <111> stress, trigonal centres divide into two groups We select <111> and <1$\bar{1}$1> directions and examine the effects of such stresses on our chosen defect, in this case that with a <111> z axis Similarly, for <110> stresses, we select the <110> and <1$\bar{1}$0> directions For <001> stresses, all trigonal centres are equivalent. In this way we arrive at the following five matrices for the case of transitions at trigonal centres

<001>

	A	Ex	Ey
A	A_1	-2B	0
Ex	-2B	A_1+2B+Δ	0
Ey	0	0	A_1-2B+Δ

<111>

	A	Ex	Ey
A	A_1+2A_2	0	0
Ex	0	$A_1'+2A_2'+\Delta$	0
Ey	0	0	$A_1'+2A_2'+\Delta$

<1$\bar{1}$1>

	A	Ex	Ey
A	$A_1-\frac{2}{3}A_2$	$\frac{2}{3}C$	$-2/\sqrt{3}\ C$
Ex	$\frac{2}{3}C$	$A_1'-\frac{2}{3}(A_2'+C)+\Delta$	$-2/\sqrt{3}\ C'$
Ey	$-2/\sqrt{3}\ C$	$-2/\sqrt{3}\ C'$	$A_1'-\frac{2}{3}(A_2'-C)+\Delta$

<110>

	A	Ex	Ey
A	A_1+A_2	B-C	0
Ex	B-C	$A_1'+A_2'-B+C+\Delta$	0
Ey	0	0	$A_1'+A_2'+B-C+\Delta$

<1$\bar{1}$0>

	A	Ex	Ey
A	A_1-A_2	B+C	0
Ex	B+C	A_1'-A_2'-B-C+Δ	0
Ey	0	0	A_1'-A_2'+B+C+Δ